

Cationic Prevesicle and Vesicle Nanoaggregates: An Experimental and Theoretical Study

Patricia del Burgo,[†] Emilio Aicart,[†] Oscar Llorca,[‡] and Elena Junquera^{*,†}

Departamento de Química Física I, Facultad de Ciencias Químicas, Universidad Complutense de Madrid, 28040-Madrid, Spain, and Centro de Investigaciones Biológicas, CSIC, Ramiro de Maeztu 9, 28040-Madrid, Spain

Received: July 19, 2006; In Final Form: September 12, 2006

The formation of spontaneous mixed prevesicles and vesicles consisting of a cationic double-chain surfactant, didecyltrimethylammonium bromide (di-C₁₀DMAB), and a cationic single-chain alkyltrimethylammonium bromide with 10 and/or 14 carbon atoms (decyltrimethylammonium bromide, C₁₀TAB, and/or tetradecyltrimethylammonium bromide, C₁₄TAB) has been investigated by means of a series of (i) highly precise experimental techniques, such as conductometry, transmission electronic microscopies (TEM and cryo-TEM), laser Doppler electrophoresis (LDE), and steady-state fluorescence spectroscopy and (ii) theoretical models, such as the DLVO theory and two of its main further modifications, Inoué's and Sogami's models. Two new potentials, based on the combination of DLVO or Inoué potentials with that of Sogami, have been proposed and checked. This theoretical analysis has been carried out not only for the aggregates studied in this work but also for other di-C_mDMAB + C_nTAB ($m = 10, 12$ and $n = 10, 12, 14$) systems previously reported by us. In respect to the experimental study, special emphasis has been devoted to the prevesicle domain. We have confirmed the existence of two critical aggregation concentrations in the very diluted concentration domain, where the conductivity plot shows a zigzag pattern: the so-called mixed critical aggregate concentration, CAC*, and the mixed critical vesicle concentration, CVC*. Contrarily, only CVC* is detected. The pre-CAC* nanoaggregates, with a variety of sizes and shapes, do not show a clear aggregation pattern, but even at such low concentrations a small number of nanoaggregates with a clear and ordered aggregation pattern has been visualized. In the postvesicle domain, the aggregates (vesicles) are unilamellar and spherical with a medium polydispersity and a net averaged surface density charge of around 14×10^{-3} (pure vesicles) and $24 \times 10^{-3} \text{ C m}^{-2}$ (mixed vesicles). The hydrophobicities of the lipidic bilayer and the surface of the vesicles resemble those of media with dielectric constants of around 30 and 75, respectively. Finally, theoretical predictions confirm the stability of the pure and mixed vesicles studied in this work and in other works previously reported.

I. Introduction

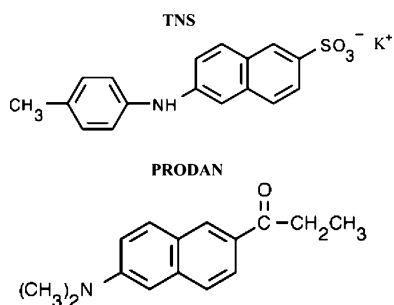
The wide variety of colloidal aggregates which results from the mixture of a double-chain surfactant, which tends to self-aggregate in vesicles, and a single-chain surfactant, for which micelles are the favored self-aggregation pattern^{1–5} is well-documented. These types of mixed colloidal systems are revealing as interesting tools not only from a practical point of view, since the conditions which determine the appearance of aggregates can be advantageously altered, but also from a scientific standpoint, since they yield a nice mosaic of different self-aggregated structures (mixed vesicles and mixed micelles, alone or coexisting, and also prevesicle nanostructures) which may transform into each other by a change in the composition of the system (surfactant relative ratio) and/or the total surfactant concentration.^{6–12} Other factors, such as the counterions (in the case of ionic surfactants), the charge, the molecular properties, and so on have an important role as well on the type, characteristics, and stability of the resulting aggregates, whether vesicles or micelles.

Several critical aggregation concentrations which are known to delimit the concentration domains within the above-mentioned aggregates may exist and/or coexist: the critical mixed vesicle concentration CVC*, the critical mixed micelle concentration CMC*, and the total critical mixed micelle concentration $\text{CMC}_{\text{tot}}^*$.^{3,6–8} The different domains could be ordered with increasing total surfactant concentration, as follows: monomers/CVC*/mixed vesicles/CMC*/mixed vesicles coexisting with mixed micelles/ $\text{CMC}_{\text{tot}}^*$ /mixed micelles. Our group has also found and confirmed that there is one more critical aggregation concentration, the so-called CAC*, below CVC*, which adds a new domain, the pre-vesicle nanoaggregates domain, and accordingly a new transition, that is, monomers/CAC*/prevesicle nanoaggregates, prior to the above-mentioned monomers/CVC*/mixed vesicles transition.^{9,12} The existence of self-aggregation prior to vesicle and/or micelle formation has been also found in the literature,^{13,14} but very few studies have been reported in this respect, probably because of the high level of requirements involved in working with precision at such extremely low concentrations and, consequently, with such low values of the experimental physicochemical property. However, we have been investigating this concentration domain along the last 3 years with a series of studies of cationic mixed systems where both the double-chain and the single-chain surfactant belong to the

[†] Universidad Complutense de Madrid.

[‡] Centro de Investigaciones Biológicas, CSIC.

* To whom correspondence should be addressed. E-mail: junquera@quim.ucm.es. Tel: +34-91-394-4131. Fax: +34-91-394-4135. <http://www.ucm.es/info/coloidal/index.html>.

CHART 1: Fluorescence Probes: TNS and PRODAN

dialkyldimethyl- and alkyltrimethylammonium bromide families.^{9,12,15} In fact, we have recently reported not only the existence of prevesicle nanoaggregates between CAC* and CVC*, but also the appearance of a kind of aggregation even below CAC*.¹² Furthermore, we could even distinguish, thanks to the high resolution of the electronic microscopy techniques, among these two kinds of prevesicle aggregates in terms of their aggregation pattern and/or structure: a disordered pattern, typical of the nanoaggregates found below CAC*, turns to an ordered fingerprint like pattern, characteristic of those found over CAC* but below CVC* and similar to the liquid crystalline phases reported for DNA-liposome complexes and/or DNA packed with viral capsid.^{16–20}

With this background, we face in the present work the complete characterization of the prevesicle and vesicle domains of a bicationic aqueous mixed colloidal system, consisting of didecyldimethylammonium bromide di-C₁₀DMAB, a commercially available cationic surfactant used as fungicidal, bactericidal, wood preservative, or disinfectant,^{21,22} and an alkyltrimethylammonium bromide with 10 (C₁₀TAB) and/or 14 carbon atoms (C₁₄TAB) on the hydrophobic chain. To carry on this study we have several highly precise experimental techniques: (i) conductometry, to determine the critical aggregation concentrations, CVC* and CAC*; (ii) transmission electron microscopy on negatively stained samples (TEM) and cryogenic transmission electron microscopy (cryo-TEM) to visualize the structure, size, shape, and morphology of the prevesicle and vesicle aggregates, respectively; (iii) laser Doppler electrophoresis (LDE) to analyze the vesicle/solution interface by means of the ζ -potential and the charge density of the aggregate surface; and (iv) steady-state fluorescence emission spectroscopy to study the different microenvironments within the inside and the surface of both the prevesicle and vesicle aggregates, by scanning the emission characteristics of two probes, the anionic probe 2-(*p*-toluidino)naphthalene-6-sulfonic acid (TNS), and/or the nonionic probe 6-propionyl-2-dimethylaminonaphthalene (PRODAN) (see Chart 1), adequately solubilized within the aggregates. To complete this characterization, we include in this work a theoretical section where several theories are used to analyze the stability of the colloidal systems experimentally studied and also that of other systems previously reported. Thus, the original DLVO theory^{23,24} and two of its main modifications, those proposed by Inoue et al.²⁵ and Sogami et al.,²⁶ applied to these systems are expected to shed light on their stability, coagulation, and flocculation regimes. Furthermore, by combining these three models we also propose in this work two new potentials in order to improve the predictions in the short-to-medium interparticle distance range. We do believe that this theoretical analysis of the dialkyldimethyl-alkyltrimethylammonium bromide mixed colloidal systems, together with the experimental results reported for them in this and in previous

works, will allow us to draw global conclusions regarding their aggregation characteristics.

II. Materials and Methods

A. Materials. The surfactants di-C₁₀DMAB and C₁₄TAB were purchased from Aldrich, and C₁₀TAB was from Fluka. The fluorescent probes, potassium salt of 2-(*p*-toluidino)naphthalene-6-sulfonic acid (TNS) and 6-propionyl-2-dimethylaminonaphthalene (PRODAN) were from Sigma and Molecular Probes, respectively. All of them, with the best purities, were used without further purification. Distilled water was deionized using a Super Q Millipore system (with a conductivity lower than 18 $\mu\text{S cm}^{-1}$) and finally was also degassed with a vacuum pump prior to the preparation of the solutions. Solutions of binary and ternary systems were prepared by mass.

B. Conductometric Measurements. Conductivity data were collected at 298.15 K (± 1 mK) with a Hewlett-Packard 4263A LCR meter. The whole equipment, the preparation of mixtures, and the fully computerized procedure was widely described previously.²⁷ The reproducibility on the specific conductivity, κ , obtained as an average of 2400 measurements for each concentration point, is better than 0.03%. The conductivity measurements were made as a function of total surfactant concentration, $[S]_{\text{tot}}$ ($= [\text{di-C}_{10}\text{DMAB}] (1) + [\text{C}_n\text{TAB}] (2)$, $n = 10$ or 14), at several constant values of the molar fraction, α_1 , defined with respect to the double-chain surfactant di-C₁₀DMAB.

C. TEM Measurements. TEM experiments were done for negatively stained samples, which were prepared following the method proposed by Kunitake and Okahata.²⁸ One milliliter of sample solution was mixed with 1 mL of 2% (w/v) uranyl acetate aqueous solutions and subsequently applied to glow-discharged copper–rhodium electron microscopy grids supporting a thin carbon film, blotted after 2 min and air-dried. Observations were conducted at a JEOL 1230 microscope operated at 100 kV. Micrographs were recorded on Kodak 4489 film at zero degrees tilt and a nominal magnification of 60000 \times under low dose conditions. Selected micrographs were digitized in a Dimage Scan Multi Pro scanner (Minolta) at 2400 dpi corresponding to a sampling window of 1.66 Å/pixel at the specimen. Sample concentrations, $[S]_{\text{tot}}$, were chosen with the help of conductivity data, considering that it must be within the range at which the prevesicle aggregates are present in solution, that is, $[S]_{\text{tot}} < \text{CVC}^*$.

D. Cryo-TEM Measurements. Samples for cryogenic transmission electron microscopy were prepared and vitrified according to the method devised by Dubochet et al.²⁹ and also described in Llorca et al.³⁰ Aliquots of 5 μL of the different samples were applied to glow-discharged carbon coated grids for 1 min, blotted for 5 s, frozen rapidly in liquid ethane at -180 °C, and kept at this temperature throughout the whole procedure using a GATAN cryo-holder and an anticontaminator. Observations were conducted at a JEOL 1230 microscope operated at 100 kV. Micrographs were recorded on Kodak 4489 film at zero degrees tilt and a nominal magnification of 30000 \times . Selected micrographs were digitalized in a Dimage Scan Multi Pro scanner (Minolta) at 2400 dpi with a final sampling window of 3.33 Å/pixel at the specimen. Sample concentrations, $[S]_{\text{tot}}$, were chosen, with the help of conductivity data, above CVC* to guarantee the presence of vesicles.

E. Electrophoretic Mobility Measurements. A laser Doppler electrophoresis (LDE) technique (Zetamaster 2000, Malvern Instruments Ltd.), previously described,⁹ was used to measure electrophoretic mobilities. The cell used is a Zetasizer 2000

standard quartz rectangular capillary electrophoresis cell of $5 \times 2 \times 50$ mm, which is calibrated with a ζ -potential transfer standard of $\zeta = -50 \pm 5$ mV. Temperature was controlled at 298.15 ± 0.01 K. Each electrophoretic mobility data is taken as an average over 10 independent measurements made at the molar fractions studied on conductivity experiments.

F. Steady-State Fluorescence Emission Spectra. Steady-state fluorescence experiments were carried out with a Perkin-Elmer LS-50B Luminescence Spectrometer.³¹ A 10 mm stoppered rectangular silica cell was placed in a stirred cuvette holder whose temperature was kept constant at 298.15 ± 0.01 K. Following a previously described procedure,¹¹ probes concentrations are kept constant at $[\text{TNS}] = 2.07 \mu\text{M}$ and/or $[\text{PRODAN}] = 5.02 \mu\text{M}$, and surfactant concentrations range from pre- to postvesicle values at each molar fraction of the ternary system. Excitation wavelengths of 330 and 340 nm were chosen, and emission wavelengths were varied from 340 to 600 nm and from 350 to 650 nm, to record the fluorescent emission of TNS and PRODAN, respectively. In all the cases, excitation and emission band slits were fixed at 2.5 nm and the scan rate selected at 240 nm/min.

G. Theoretical Overview. DLVO Theory. Formulated by Derjaguin and Landau²³ and Verwey and Overbeek,²⁴ the well-known DLVO theory states that the interaction among two colloidal particles results from the balance between attractive dispersion forces (London or van der Waals forces) and repulsive electrostatic forces (owing to the overlapping of electric interfaces). It evaluates this interaction as a function of the distance, as briefly summarized next. The stability of colloidal aggregates depends on the total interaction energy, V_T , which, for spherical aggregates of equal radius a at a distance H , is expressed as^{32–35}

$$V_T(H) = V_R(H) + V_A(H) = \frac{64\pi a n^0 k_B T}{\kappa_D^2} \Gamma^2 \exp(-\kappa_D H) - \frac{Aa}{12H} \quad (1)$$

where $V_R(H)$ and $V_A(H)$ are the interaction energies due to electrostatic repulsion and attractive dispersion, respectively, κ_D the inverse of the Debye length, n^0 the number of ions per volume, Γ a constant depending on the potential energy and temperature, and A is the Hamaker constant.^{34–36} As a result of the above shown dependency with H , attraction is dominant for small distances (primary minimum), while repulsion may be dominant at longer distances.³⁴ Sometimes, a potential barrier at H_{\max} and a secondary minimum appears; both features are important when analyzing the colloidal stability. The attractive energy depends on the particle Hamaker constant and cannot be modified, but the repulsive energy, which depends on the Stern layer potential and/or on κ_D^{-1} , can be altered by, for example, changing the ionic strength. Furthermore, above a certain electrolyte concentration, known as *critical coagulation concentration*, CCC, the energy barrier falls below zero, and the particles then coagulate rapidly.

For many years, DLVO theory has constituted a solid basis to describe the colloidal stability, but it cannot satisfactorily explain several behaviors, mainly, in concentrated colloidal suspensions, in systems with high surface potential, ψ_0 , or in the case of big colloidal particles. In the years that followed the first development of the theory, several models came up with the aim of overcoming its main failures, among which we want to emphasize in this work the models proposed by Inoue²⁵ and Sogami.²⁶

Inoue's Model. Inoue et al.²⁵ combines the DLVO electrostatic potential with an expression derived by Hogg³⁷ to build the electrostatic repulsive term, $V_R(H)$, which, for two spherical colloidal particles, results

$$V_R(H) = \frac{\epsilon a \psi_0^2}{2} \ln[1 + \exp(-\kappa_D H)] \quad (2)$$

where ϵ is the dielectric constant of the medium, and ψ_0 the surface potential of the particle. On the other hand, this model uses the following expression, derived by Vold,³⁸ to build the attractive interaction potential, also for spherical particles:

$$V_A(H) = -\frac{A_{232}}{12} (F_{11} + F_{22} - 2F_{12}) \quad (3)$$

where A_{232} is the effective constant of Hamaker and F_{ii} is given by

$$F_{ii} = \frac{y}{x^2 + xy + x} + \frac{y}{x^2 + xy + x + y} + 2 \ln \left[\frac{x^2 + xy + x}{x^2 + xy + x + y} \right] \quad (4)$$

where x and y are related with H , a , and the interface thickness, d_{dc} , through the following relations:

$$\text{For } F_{11}: \quad y = 1 \quad x = (H + 2d_{dc})/2(a - d_{dc}) \quad (5)$$

$$\text{For } F_{22}: \quad y = 1 \quad x = H/2a \quad (6)$$

$$\text{For } F_{12}: \quad y = a/(a - d_{dc}) \quad x = (H + d_{dc})/2(a - d_{dc}) \quad (7)$$

Combining eqs 2 and 3, the resulting total interaction potential proposed by Inoue's model is

$$V_T(H) = \frac{\epsilon a \psi_0^2}{2} \ln[1 + \exp(-\kappa_D H)] - \frac{A_{232}}{12} (F_{11} + F_{22} - 2F_{12}) \quad (8)$$

It has been mainly used for checking the colloidal stability of a wide variety of systems, mostly at high ionic strength.²⁵

Sogami's Model. This model proposes that not only a medium-range repulsion term but also a long-range weak attractive interaction term should be included to estimate the overall electrostatic interaction between the particles.^{26,39} This attractive interaction normally drives to a secondary minimum in the total potential at a distance H_{\min} , which is outside of the attractive van der Waals range, this secondary minimum being the responsible of the flocculation phenomena. Briefly, Sogami's model calculates the total electrostatic energy, E_T , as a function of the position of the particles by integrating over the total volume, V , as follows:

$$E_T = \frac{1}{2} \sum_i Z_i e \int \psi(r) \rho_i(r) dV + \frac{1}{2} \int \psi(r) \left[-\frac{\epsilon \kappa_D^2}{4\pi} \phi(r) \right] dV \quad (9)$$

where the first term represents the electrostatic energy of all particles in the field of potential $\psi(r)$ and the second term is the electrostatic energy referred only to the counterions; $\phi(r)$ is defined as a shifted potential field with respect to $\psi(r)$ and $\epsilon \rho_i$

(r) is the true charge density in the solution. This last term is responsible of the attractive electrostatic force among the particles.

Sogami et al. obtained free Gibbs energy, G , from the total electrostatic energy, E_T , and the Helmholtz free energy, F , by the expression

$$G = G^0 + \frac{1}{2} \sum_{m \neq l} U_{ml}^G + \sum_l V_l^G \quad (10)$$

where G^0 is the free Gibbs energy in the limit of $e^2 = 0$. The adiabatic potential, U_{ml}^G , that only depends on the relative configuration and orientation of two particles l and m , and the adiabatic potential of a particle n due to the ions around it, V_l^G , is obtained by

$$U_{ml}^G = \frac{(Ze)^2}{\epsilon} \left[\frac{\sinh(\kappa_D a)}{\kappa_D a} \right]^2 \left[1 + \kappa_D a \coth(\kappa_D a) - \frac{1}{2} \kappa_D R_c \right] \frac{\exp(-\kappa_D R_c)}{R_c} \quad (11)$$

$$V_l^G = \frac{(Ze)^2}{4\epsilon a} \left[\frac{1 - \exp(-2\kappa_D a)}{2\kappa_D a} + \exp(-2\kappa_D a) \right] + \frac{(Ze)^2}{2\epsilon a} \left[\frac{1 - \exp(-2\kappa_D a)}{2\kappa_D a} \right] \quad (12)$$

where $R_c (= H + 2a)$ is the distance between the centers of the two particles and Ze the charge density of the colloidal particle.

The U_{ml}^G potential, which reflexes the effective attraction among the particles at long distances, is the Sogami's potential, from now on V_T . It shows a minimum at

$$R_{c,\min} = (H + 2a)_{\min} = \frac{C + 1 + [(C + 1)(C + 3)]^{1/2}}{\kappa_D} \quad (13)$$

where C is defined by

$$C = \kappa_D a \coth(\kappa_D a) \quad (14)$$

This model, which predicts that ionic particles repulse each other at short distances, while attract each others at longer distances, has been mainly applied to analyze the colloidal stability of latex particles.²⁶

III. Results and Discussion

The characterization of the vesicle and prevesicle mixed aggregates consisting of di- C_{10} DMAB and a cationic single-chain surfactant of either 10 or 14 carbon atoms of the alkyltrimethylammonium bromide family, via electronic microscopy techniques (to know the size, morphology, and shape of the aggregates), spectroscopic techniques (to elucidate the polarity of the bilayer and of the surface of the aggregates), and electrophoretic techniques (to calculate their surface charge density) is supported on the determination of the critical aggregation concentrations, which limit the concentration regions where these mixed aggregates may exist. These critical aggregation concentrations, both CAC* (monomers to mixed prevesicle aggregates transition) and CVC* (mixed prevesicle to mixed vesicle aggregates transition) have been determined at several molar fractions, α_1 , of the mixed systems from the plots of specific conductivity versus total surfactant concentrations, following the third derivative method (Phillip's plot).⁴⁰

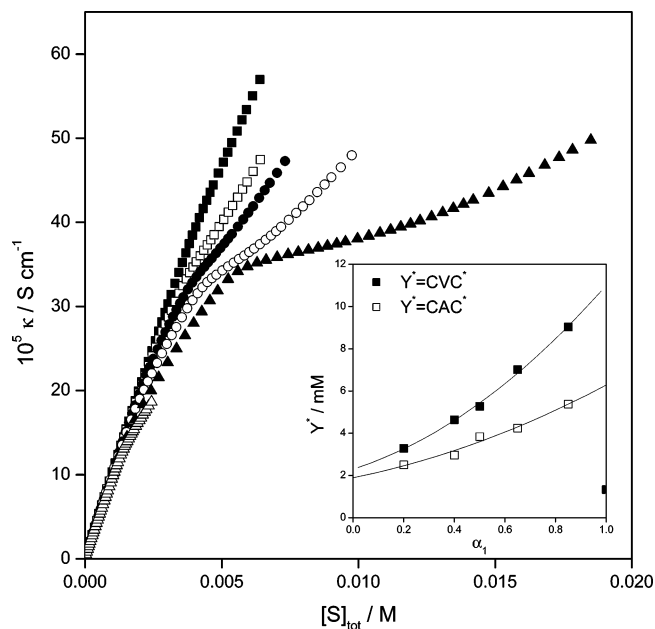


Figure 1. Plot of specific conductivity κ as a function of total surfactant concentration $[S]_{\text{tot}}$, in the very diluted range, at 298.15 K and constant molar fraction α_1 for the mixed system di- C_{10} DMAB + C_{10} TAB: ■, $\alpha_1 = 0.200$; □, $\alpha_1 = 0.401$; ●, $\alpha_1 = 0.500$; ○, $\alpha_1 = 0.650$; ▲, $\alpha_1 = 0.850$; and △, $\alpha_1 = 1$. The inset shows a plot of CVC* (solid symbols) and CAC* (open symbols) as a function of the molar fraction, α_1 .

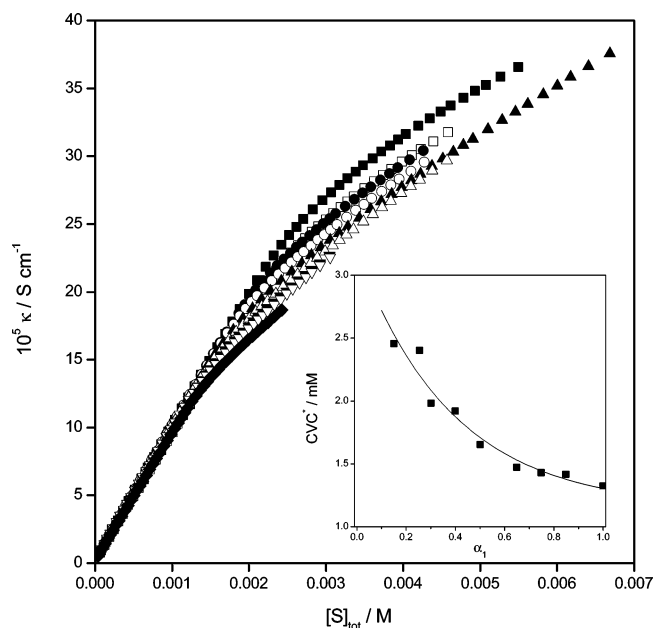


Figure 2. Plot of specific conductivity κ as a function of total surfactant concentration $[S]_{\text{tot}}$, in the very diluted range, at 298.15 K and constant molar fraction α_1 for the mixed system di- C_{10} DMAB + C_{14} TAB: ■, $\alpha_1 = 0.150$; □, $\alpha_1 = 0.254$; ●, $\alpha_1 = 0.301$; ○, $\alpha_1 = 0.399$; ▲, $\alpha_1 = 0.500$; △, $\alpha_1 = 0.649$; ▼, $\alpha_1 = 0.749$; ▽, $\alpha_1 = 0.848$; and ◆, $\alpha_1 = 1$. The inset shows a plot of CVC* as a function of the molar fraction, α_1 .

Figures 1 and 2 show the experimental conductivity data in the very diluted concentration range for the mixed systems studied in this work, and Table 1 summarizes the resulting critical concentrations. The insets of these figures show the plot of the critical aggregation concentrations vs the molar fraction of the system. The pattern followed by both systems, di- C_{10} DMAB/ C_{10} TAB and di- C_{10} DMAB/ C_{14} TAB, in both plots, κ versus $[S]_{\text{tot}}$ and CAC* or CVC* versus α_1 , is in agreement with what we have been observing in other systems previously studied.^{9,12,15}

TABLE 1: Values of CAC* and CVC* at Several Molar Fractions, α_1 , of the Mixed System Di-C₁₀DMAB + C_{*n*}TAB, with *n* = 10 and 14^a

α_1	<i>n</i> = 10 C ₁₀ TAB		α_1	<i>n</i> = 14 C ₁₄ TAB	
	CAC* (mM)	CVC* (mM)		CVC* (mM)	
			0.150	2.46	
0.200	2.50	3.28	0.254	2.40	
0.401	2.96	4.64	0.301	1.98	
0.500	3.83	5.27	0.399	1.92	
0.650	4.24	7.01	0.500	1.65	
0.850	5.37	9.03	0.649	1.47	
			0.749	1.43	
			0.848	1.42	
1		1.33	1	1.33	

^a Error on critical concentrations are (± 0.01).

When the conductivity plot shows a zigzag pattern, at least at high molar fractions (Figure 1), the CAC* or CVC* versus α_1 plot is like that one shown in the inset of Figure 1, that is, both aggregation concentrations increase with the molar fraction of the system, but when the zigzag pattern does not appear, which means that CAC* cannot be detected (Figure 2), CVC* is found to decrease with the molar fraction of the system, tending to the value of CVC for the pure double-chain surfactant (see the inset in Figure 2). This conclusion is supported by this work and those previously reported by us.^{9,12,15} We have stated our belief with respect to these two possible behaviors: the occurrence of the zigzag on conductivity plots, which means that there is a detectable concentration range within which the ordered prevesicle aggregates exist, does depend on whether the critical concentrations CVC and CMC are close to each other or not. When these critical concentrations are enough separated (in concentration units), the zigzag is detected, while the contrary is true when they are close. Figure 3, which shows the referred conductivity plots at the equimolecular molar fraction for the systems studied herein and those previously reported,^{9,12,15} clearly supports this conclusion. Also in the figure is included the data for the system di-C₁₀DMAB/C₁₆TAB at $\alpha_1 = 0.5$, measured in this work to complete this figure. Notice that di-C₁₂DMAB/C_{*n*}TAB mixed systems show the zigzag except for *n* = 16 (CVC and CMC are very close to each other), while di-C₁₀DMAB/C_{*n*}TAB only shows this zigzag for *n* = 10, which is the unique case where CVC and CMC are apart from each other.

The shape, size, and morphology of the mixed aggregates studied in this work have been evaluated by using transmission electron microscopy techniques. For that purpose, TEM experiments were done for two negatively stained samples for each molar fraction: (i) a blank or control sample at $[S]_{\text{tot}} = 0$, consisting on a 1:1 mixture of aqueous solution and uranyl acetate, treated with the same protocol as the working sample; and (ii) a sample at $[S]_{\text{tot}}$ below CVC*, which is the prevesicle domain. As expected, a continuous background is seen in micrographs of the control samples; however, TEM micrographs for samples with $[S]_{\text{tot}} < \text{CVC}^*$, show (i) an appreciable number of aggregates of variable shapes and sizes, without a defined and clear aggregation pattern and/or structure and (ii) a low number of spherical aggregates with a clear ordered fingerprint pattern. Both types of aggregates were already found in a previous work;¹² as there, we will refer to them as disordered and ordered prevesicle aggregates, which are pointed by asterisks and arrows, respectively, in Figure 4a, that shows as an example images of such prevesicle aggregates for the di-C₁₀DMAB/C₁₀-

TAB mixed system at $\alpha_1 = 0.500$. Similar TEM micrographs were found for di-C₁₀DMAB/C₁₄TAB at the same molar fraction. The disordered (asterisks) and ordered aggregates (arrows) are seen with amplification in Figure 4 (panels b and c). As can be noticed, the ordered structures of Figure 4c are arranged as circles of various diameters and are made of an internal collection of slices. To analyze the regular arrangement of these ring-shaped aggregates, a well-defined ring for each case was selected, and a line was drawn across the image to plot the intensities of the gray levels for each pixel along the line (see Figure 4d). The number of pixels between several contiguous peaks were then calculated and found to follow a regular pattern of 18 and 19 pixels on average for di-C₁₀DMAB/C₁₀TAB (shown in the figure) and di-C₁₀DMAB/C₁₄TAB (not shown) aggregates, respectively. This value was multiplied by the 0.166 nm per pixel at the specimen after digitization of the micrographs, which yielded a spacing of approximately 3.1 and 3.2 nm between repetitive elements of the ordered prevesicle aggregates found in the mixed systems above-mentioned, respectively. These results are in very good agreement with those found for di-C₁₂DMAB/C_{*n*}TAB mixed prevesicle aggregates, previously reported,^{9,10,12} indicating that the length of the double-chain surfactant does not affect the structural characteristics of the aggregates formed prior to appearance of the mixed vesicles. Furthermore, this fingerprint pattern is similar to that one found in the literature for DNA molecules packed within cationic liposomes (known as genosomes)^{16–19} and/or viral capsids.²⁰ This pattern has been additionally resolved in some of these works by Fourier transform techniques into diffraction images which pointed to inverted hexagonal H_{II}^{C} phases.^{16,18,41,42} These Fourier techniques have been also applied on the images obtained in this work, but the inverted hexagonal phase was not found. Further studies in this sense will be welcomed. Finally, the same image processing protocol was also applied to several images corresponding to the prevesicle aggregates pointed by asterisks in Figure 4a and amplified in Figure 4b, but a clear pattern with a defined spacing was not found in this case, confirming the disordered character of these aggregated structures. These results corroborate what we have recently reported as clear evidence of (i) the existence of aggregates below CVC* and even below CAC*, that is, within a concentration region where only monomers were supposed to exist, and (ii) a noticeable difference in terms of structure and packing characteristics among these prevesicle aggregates.

Cryo-TEM experiments were run on one sample for each molar fraction at $[S]_{\text{tot}}$ above CVC*, where mixed vesicles are present. Figure 5 shows an example of the micrographs taken on cryo-TEM experiments of di-C₁₀DMAB/C₁₀TAB (a) and di-C₁₀DMAB/C₁₄TAB (b) at $\alpha_1 = 0.500$. These photographs revealed the presence of unilamellar spherical vesicles, with an average diameter of around (33 ± 7) nm in both systems, in agreement with other cationic mixed vesicles previously studied.¹²

The compounds with an electron donor–acceptor moiety linked by a single bond to an aromatic ring, like TNS and PRODAN (see Chart 1), possess characteristic spectroscopic properties, which have been widely explained in the literature.^{43,44} It is known⁴⁴ that the ground states of the fluorescent probes used in this work yield, upon excitation, a locally excited state (LE) (via $\pi \rightarrow \pi^*$ electronic transition). The mechanism by which this excited state is formed and deactivated has been interpreted by using different approaches.^{43–50} In this work, we have followed that approach⁵⁰ that considers the $\pi \rightarrow \pi^*$ emission band of the fluorescent probe as consisting on different

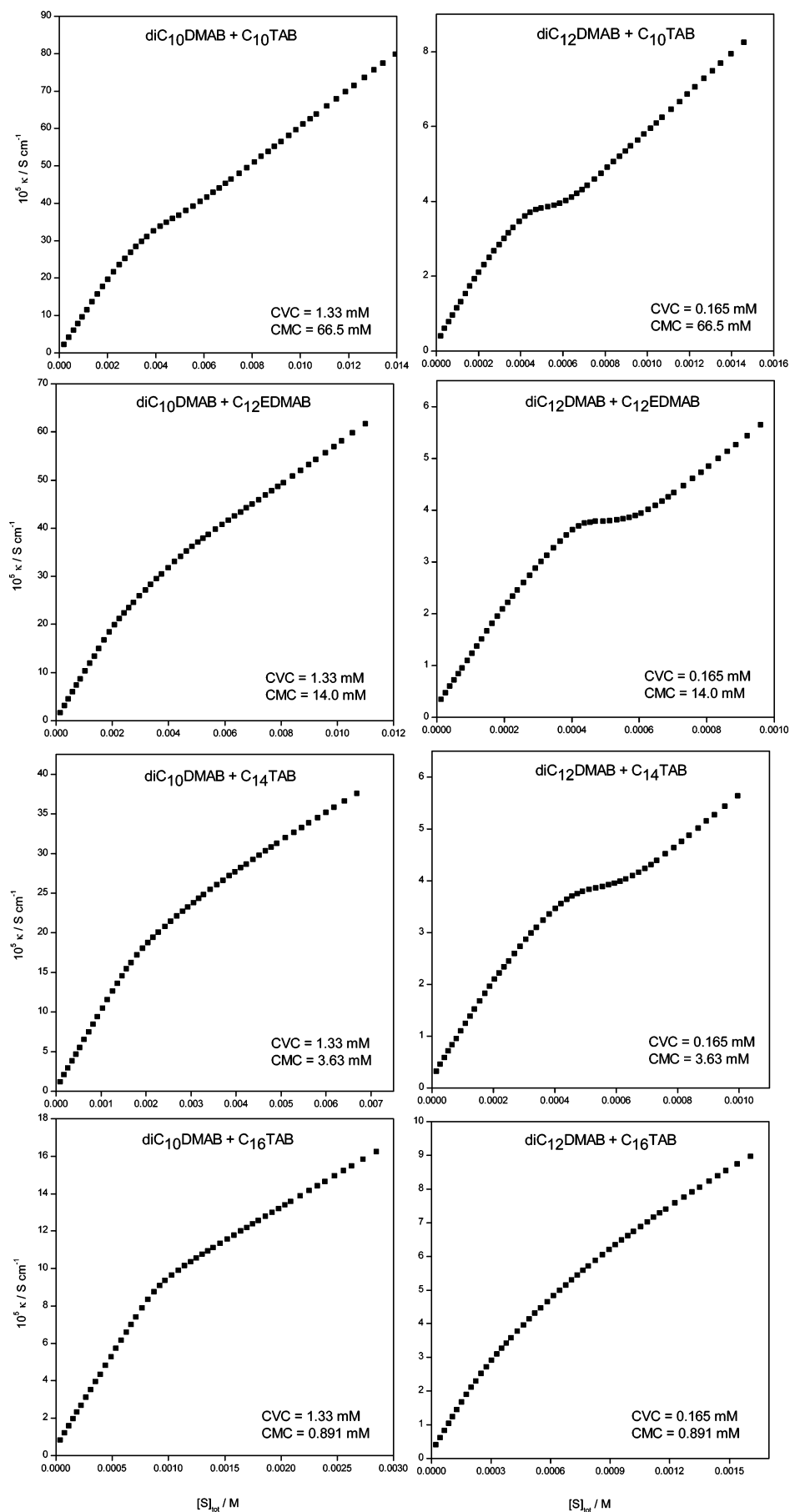


Figure 3. Plot of specific conductivity κ as a function of total surfactant concentration $[S]_{\text{tot}}$, in the very diluted range, at 298.15 K at constant molar fraction α_1 around 0.5 for the mixed systems consisting of di- C_{10}DMAB and C_{10}TAB , di- C_{10}DMAB and $\text{C}_{12}\text{EDMAB}$ (ref 15), di- C_{10}DMAB and C_{14}TAB , di- C_{10}DMAB and C_{16}TAB , di- C_{12}DMAB and C_{10}TAB (ref 12), di- C_{12}DMAB and $\text{C}_{12}\text{EDMAB}$ (ref 9), di- C_{12}DMAB and C_{14}TAB (ref 12) or di- C_{12}DMAB and C_{16}TAB (ref 12).

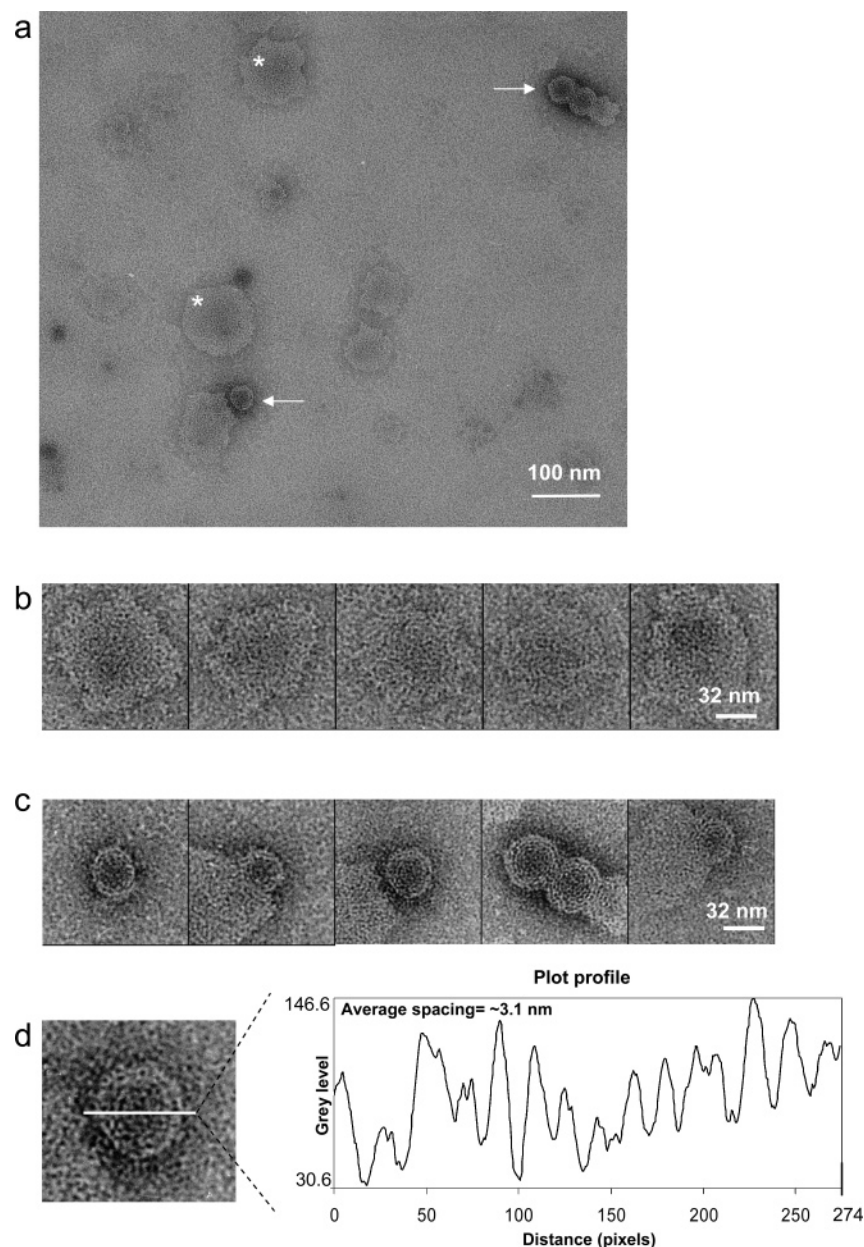


Figure 4. (a) TEM field of a di- C_{10} DMAB + C_{10} TAB solution at $\alpha_1 = 0.500$ and $[S]_{\text{tot}} = 2.367$ mM after negative staining with uranyl acetate. (Scale bar: 100 nm.) Asterisks and arrows point to disordered and ordered prevesicle aggregates, respectively; (b and c) The images pointed by asterisks (disordered aggregates) and arrows (ordered aggregates) shown in panel a are magnified to highlight the structural details within the aggregates. (Scale bar: 32 nm); (d) 2D image of a characteristic fingerprint pattern corresponding to an ordered prevesicle aggregate, revealing and highlighting that the aggregates are made of a repetitive unit of around 3.1 nm in section, as clearly shown in the plot of the gray levels along a straight line across the 2D image. The maximum densities are revealed as peaks within a distance of 18 pixels, corresponding to 3.1 nm (0.17 nm per pixel after the scanning of the micrographs).

bands at different wavelengths, each of which is attributable to the $\pi \rightarrow \pi^*$ emission of the probe immersed within different aggregate microenvironments, characterized by its hydrophobicity, microviscosity, rigidity, and/or solvation features. Figure 6 shows the emission spectra of TNS and PRODAN for a series of di- C_{10} DMAB/ C_{10} TAB/probe and di- C_{10} DMAB/ C_{14} TAB/probe aqueous solutions at different molar fractions, α_1 , and total surfactant concentration, $[S]_{\text{tot}}$. These concentrations were chosen to have either prevesicle aggregates or vesicles, according to the CVC* values previously obtained from conductivity experiments. Experimental emission spectra were analyzed by deconvolution into overlapping Gaussian curves with a commercial nonlinear least-squares multi-peaks fitting procedure (implemented in Microcal Origin version 7.0383) that uses an iterative Marquardt–Levenberg fitting algorithm. Both the

procedure and the control of the goodness of the fits were widely explained elsewhere.¹¹ Figure 7 shows, as examples, the deconvolutions of TNS and PRODAN emissions for the mixed systems studied herein at $\alpha_1 = 0.5$, while Tables 2 and 3 summarize the fitting parameters.

As can be observed both in Figure 7 and in Tables 2 and 3, the mathematical treatment points in all the cases to the presence of three microenvironments, which is the pattern usually found by us for other mixed colloidal systems previously reported.^{11,12,51} Also in common is the fact that the emission bands due to TNS immersed within prevesicle microenvironments (dashed lines in Figure 6 (panels a and c)) are blue shifted with respect to those due to TNS immersed within vesicle microenvironments (solid lines in Figure 6 (panels a and c)), while the contrary is true for PRODAN (see Figure 6 (panels b and d)).

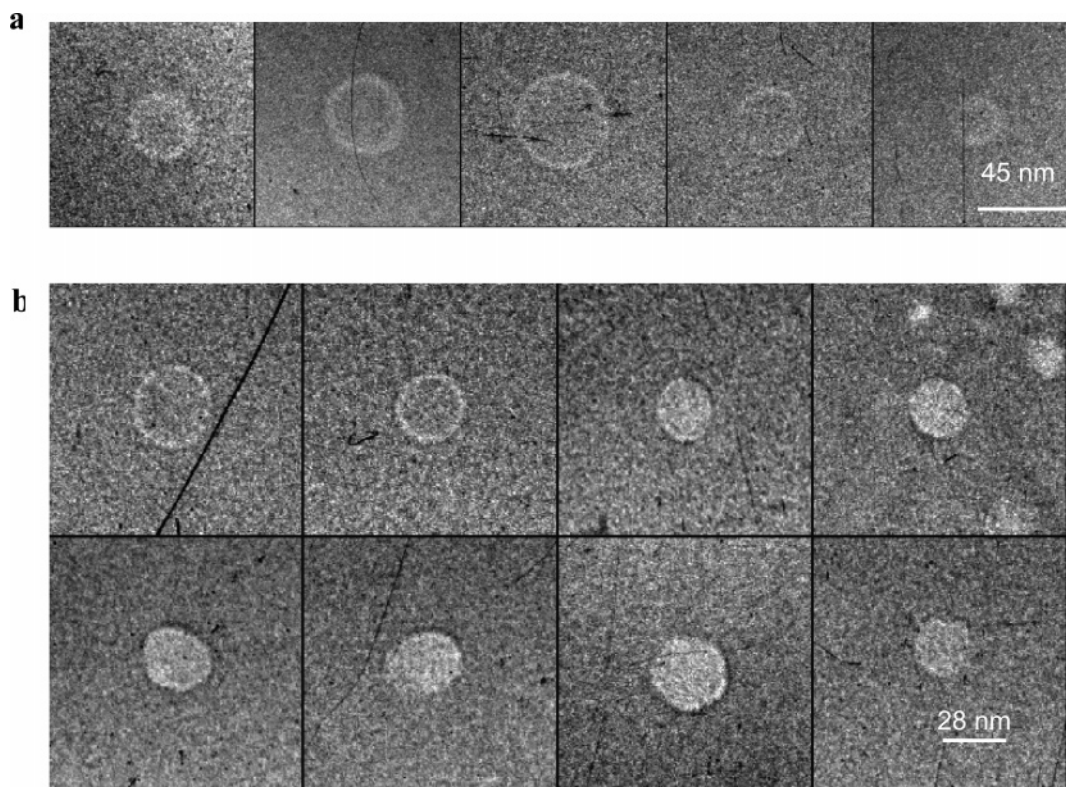


Figure 5. A gallery of selected cryo-TEM images of mixed vesicles corresponding to (a) a di- C_{10} DMAB + C_{10} TAB solution at $\alpha_1 = 0.500$ and $[S]_{\text{tot}} = 7.319$ mM. (Scale bar: 45 nm); and (b) a di- C_{10} DMAB + C_{14} TAB solution at $\alpha_1 = 0.500$ and $[S]_{\text{tot}} = 2.307$ mM. (Scale bar: 28 nm.)

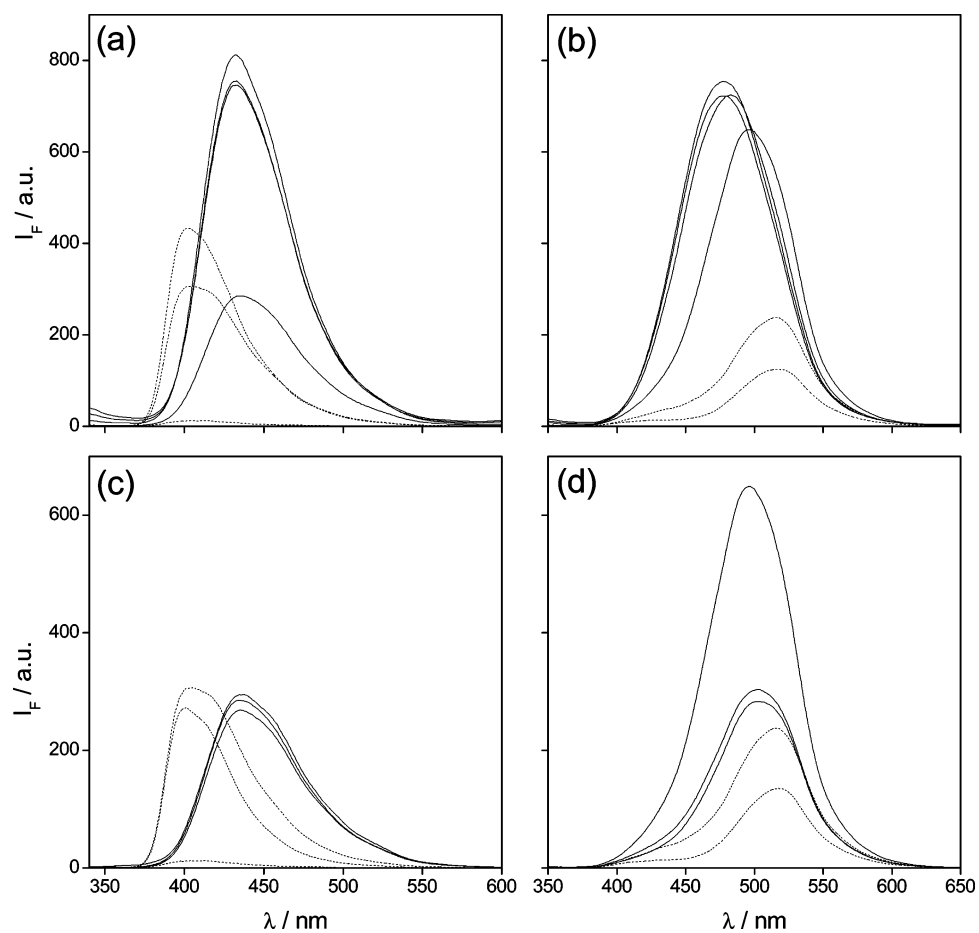


Figure 6. Steady-state emission fluorescence spectra of (a, c) TNS ($[TNS] = 2.07 \mu\text{M}$) and (b, d) PRODAN ($[PRODAN] = 5.02 \mu\text{M}$) immersed on aqueous solutions of di- C_{10} DMAB + C_{10} TAB (a, b) and di- C_{10} DMAB + C_{14} TAB (c, d), respectively. Dash and solid lines correspond to prevesicle and vesicle concentrations, respectively.

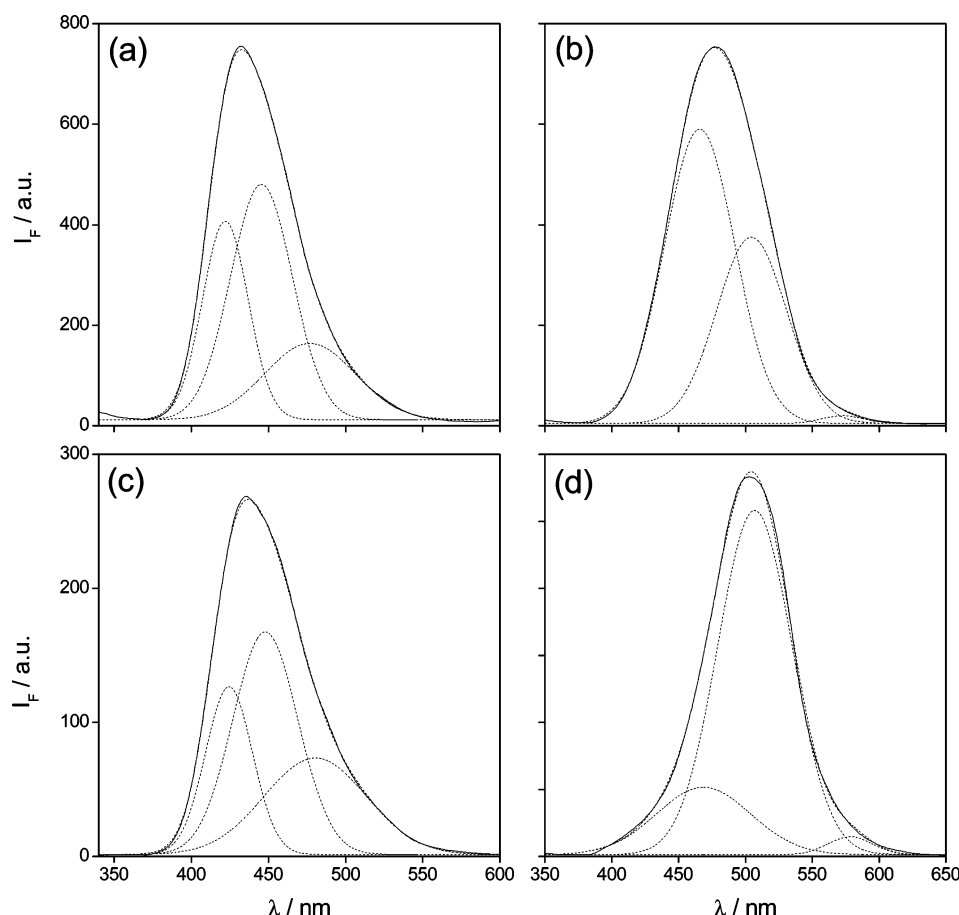


Figure 7. Deconvolution of the emission fluorescence band of TNS (a, c) immersed on a vesicle solution of (a) di-C₁₀DMAB + C₁₀TAB ($\alpha_1 = 0.500$, $[S]_{\text{tot}} = 11.698$ mM) and (c) di-C₁₀DMAB + C₁₄TAB ($\alpha_1 = 0.500$, $[S]_{\text{tot}} = 2.079$ mM); and PRODAN (b, d) immersed on a vesicle solution of (b) di-C₁₀DMAB + C₁₀TAB ($\alpha_1 = 0.500$, $[S]_{\text{tot}} = 11.728$ mM) and (d) di-C₁₀DMAB + C₁₄TAB ($\alpha_1 = 0.500$, $[S]_{\text{tot}} = 2.090$ mM).

TABLE 2: Parameters of the Deconvoluted Gaussian Bands of the TNS and PRODAN Fluorescence Emission Spectra at Various Molar Fractions, α_1 , and Total Surfactant Concentrations, $[S]_{\text{Tot}}$, of the Mixed System Di-C₁₀DMAB + C₁₀TAB^a

α_1	$[S]_{\text{tot}}$ mM	CVC* mM	$[S]_v$ mM	λ_{max} nm	I_{max}	λ_1 nm	A_1 %	W_1	λ_2 nm	A_2 %	W_2	λ_3 nm	A_3 %	W_3	r^2
PROBE = TNS															
0.500	0.699	5.27		399.5	455.7	396.4	21.2	17	414.0	44.0	29	441.4	34.8	52	0.9988
1	0.070	1.33		416.1	17.7	397.1	17.8	20	414.5	49.4	33	445.3	32.8	59	0.9986
1	0.696	1.33		401.5	314.1	396.3	17.3	16	415.1	42.5	30	443.9	40.2	54	0.9985
0.500	7.300	5.27	2.030	433.0	827.0	422.1	29.9	29	446.0	47.3	40	476.7	22.8	61	0.9999
0.500	11.70	5.27	6.428	433.5	771.2	422.0	29.7	29	445.5	47.9	40	476.8	22.4	58	0.9998
0.651	13.41	7.01	6.407	431.4	764.6	422.5	31.3	30	446.7	50.5	40	482.0	18.2	54	0.9996
1	3.113	1.33	1.788	436.5	292.9	424.0	23.6	30	447.4	47.2	43	479.7	29.2	66	0.9999
PROBE = PRODAN															
0.500	0.698	5.27		519.0	133.7	435.3	9.2	55	515.0	86.5	50	576.5	4.3	34	0.9993
1	0.700	1.33		514.5	247.0	459.6	20.0	66	514.7	75.5	49	576.0	4.6	36	0.9993
0.500	7.319	5.27	2.049	483.1	733.8	471.9	70.4	57	511.0	28.2	49	571.9	1.4	34	0.9999
0.500	11.728	5.27	6.459	479.5	776.0	465.8	60.9	53	504.6	38.2	52	572.8	0.9	30	0.9999
0.650	13.450	7.01	6.445	478.0	736.0	466.2	62.6	53	505.0	36.5	51	571.2	0.9	29	0.9999
1	3.122	1.33	1.796	495.1	664.8	440.2	6.8	51	498.7	91.6	59	578.9	1.6	30	0.9996

^a Wavelength λ_i , width W_i , and area A_i in terms of % contribution to the overall fluorescence emission area. CVC* and $[S]_v$ are the mixed critical vesicle concentration and the surfactant concentration on vesicle form.

The criteria followed for assigning these experimental bands to different microenvironments is well-known:^{43,44} the more hydrophobic the probe solubilization site is, the more blue shifted its emission maximum λ becomes. Thus, we have found^{11,12} that these probes may solubilize within the hydrophobic bilayer and/or the surface of the mixed vesicles. Nevertheless, considering the structure of TNS and PRODAN, which have hydrophilic groups, even when the probes are immersed within the hydrophobic bilayer, they may remain in part in contact with the vesicle palisade. Prevesicle assemblies also offer the probes

solubilization sites of variable hydrophobicity; in fact, we have even distinguished among the ordered prevesicle nanoaggregates (fingerprint like pattern), which behave as vesicles, and the disordered prevesicle nanoaggregates, which usually present two types of microenvironments, their inside and a kind of loose clusters within which the probe may experience a less apolar surrounding due to a certain water penetration.¹² The association of a fluorescent probe with, for example, monomers or clusters of surfactant in aqueous media, responsible for the emission observed at concentrations below the critical aggregation

TABLE 3: Parameters of the Deconvoluted Gaussian Bands of the TNS and PRODAN Fluorescence Emission Spectra at Various Molar Fractions, α_1 , and Total Surfactant Concentrations, $[S]_{\text{Tot}}$, of the Mixed System Di-C₁₀DMAB + C₁₄TAB^a

α_1	$[S]_{\text{Tot}}$ mM	CVC* mM	$[S]_v$ mM	λ_{max} nm	I_{max}	λ_1 nm	A_1 %	W_1	λ_2 nm	A_2 %	W_2	λ_3 nm	A_3 %	W_3	r^2
PROBE = TNS															
0.500	0.696	1.65		398.0	287.1	395.3	21.1	16	412.2	46.2	28	437.4	32.7	48	0.9991
1	0.070	1.33		416.1	17.7	397.1	17.8	20	414.5	49.4	33	445.3	32.8	59	0.9986
1	0.696	1.33		401.5	314.1	396.3	17.3	16	415.1	42.5	30	443.9	40.2	54	0.9985
0.500	2.079	1.65	0.425	434.8	274.6	424.4	24.6	30	448.0	45.1	42	480.3	30.4	66	0.9999
0.649	1.895	1.47	0.423	436.5	307.9	426.5	33.3	32	453.5	24.1	35	469.8	42.6	71	0.9999
1	3.113	1.33	1.788	436.5	292.9	424.0	23.6	30	447.4	47.2	43	479.7	29.2	66	0.9999
PROBE = PRODAN															
0.500	0.702	1.65		519.4	141.2	440.2	9.1	58	515.2	85.9	49	575.6	5.0	34	0.9990
1	0.700	1.33		514.5	247.0	459.6	20.0	66	514.7	75.5	49	576.0	4.6	36	0.9993
0.500	2.090	1.65	0.436	502.0	290.6	468.8	19.4	70	507.0	78.2	55	578.4	2.4	33	0.9995
0.649	1.886	1.47	0.413	502.0	315.8	458.8	17.4	65	505.6	80.3	56	578.6	2.3	32	0.9995
1	3.122	1.33	1.796	495.1	664.8	440.2	6.8	51	498.7	91.6	59	578.9	1.6	30	0.9996

^a Wavelength λ_i , width W_i , and area A_i in terms of % contribution to the overall fluorescence emission area. CVC* and $[S]_v$ are the mixed critical vesicle concentration and the surfactant concentration on vesicle form.

concentration, is already documented in the literature.^{13,14} Furthermore, it is known that some probes hardly fluoresce in water, but they do in aqueous solutions with small amounts of surfactant (below CVC or CMC).¹³ It means that in prevesicle solutions, the probe must be within environments with less polarity than water. And, obviously, whether in the presence of vesicles or prevesicles (ordered or disordered), there is always a third microenvironment where the probe may be housed, the bulk, whose characteristic emission band would probably be expected to be the most red shifted one, since it seems to be the most polar site among all the microenvironments above-mentioned. Actually, this is the emission pattern found for nonionic PRODAN immersed in vesicles or prevesicles of bicationic mixed colloidal systems. However, the anionic TNS behaves differently when vesicles are present, in the sense that it experiences a lower energy transition when it is housed in the surface, than when it is in the bulk, indicating that the charged double-chain surfactant heads yield a more polar microenvironment than that of the bulk in this case. Consequently, the order expected for the emission bands which results from the deconvolution operation would be (i) pre-vesicles, λ (inside) < λ (within clusters) < λ (bulk) for both nonionic PRODAN and anionic TNS and (ii) vesicles, λ (bilayer) < λ (bulk) < λ (surface) for TNS and λ (bilayer) < λ (surface) < λ (bulk) for PRODAN, as will be confirmed next for the systems studied in this work.

The Gaussian components obtained for the prevesicle aggregate solutions of both systems are centered at around 396, 414, and 445 nm (first three lines in Tables 2 and 3) for TNS and at around 445, 515, and 576 nm (first two lines in Tables 2 and 3) for PRODAN, whereas those for vesicle solutions are centered at around 424, 445, and 477 nm and at around 460, 505, and 576 nm for TNS and PRODAN, respectively, as well. With the above-mentioned general considerations, we have assigned these emission bands, as follows. Since the emission of TNS at around 445 nm and that of PRODAN at 576 nm are the unique bands in common for vesicle and prevesicle solutions in each case, they have been assigned to the probe in the bulk. In the presence of prevesicle aggregates, the emission bands have been assigned to the probe housed within the aggregates (396 nm for TNS and 445 nm for PRODAN) and to the probe placed within the aqueous regions surrounded by regions of aggregates or clusters (414 nm for TNS and 515 nm for PRODAN). In the presence of vesicles, the emissions at around 424 and 460 nm have been attributed to the probe (TNS and PRODAN, respectively) in the hydrophobic bilayer, whereas

the emissions at 477 and 505 nm have been assigned to the probes in the vesicle surface. It can be noticed that these results meet the above-mentioned general patterns, which can be confirmed as characteristics of the interaction of a molecular fluorescence probe and bicationic mixed colloidal systems consisting of a dialkyldimethylammonium bromide and an alkyltrimethylammonium bromide surfactant.^{12,51}

The above assigned λ_i values can be compared with the reported λ_{max} values of TNS and PRODAN in a series of pure solvents of known dielectric constant.^{43,52} Thus, the results obtained in the case of TNS would indicate that the hydrophobic core of di-C₁₀DMAB/C₁₀TAB or di-C₁₀DMAB/C₁₄TAB vesicles presents a polarity similar to that of a C₃–C₄ alcohol with ϵ around 20, while that of the vesicle surface is intermediate between the characteristic polarities of ethylenglycol and/or formamide (with $\epsilon = 76$) microenvironments. On the other hand, the results obtained from PRODAN spectra reveal a vesicle hydrophobic core similar to dimethylformamide ($\epsilon = 37$) and a surface with a polarity close to that of deuterium oxide, with $\epsilon = 78$. Considering that the vesicles are the same in both cases, it could be concluded that the vesicles studied in this work have a bilayer and a surface with hydrophobicities corresponding to dielectric constants of around 30 (± 5) and around 75 (± 5), respectively.

Once the different microenvironments are identified and assigned to wavelengths, attention can be paid to the interesting information yielded by the intensity of the bands in terms of the areas (which are expressed as percentages over the total area of the experimental band). It is worth noticing that both probes are predominantly solubilized within the vesicles, that is, $(A_1 + A_3) > A_2$ for TNS and $(A_1 + A_2) > A_3$ for PRODAN, as can be seen in Tables 2 and 3, irrespective of the length of the single-chain surfactant tail. In the case of di-C₁₀DMAB/C₁₄TAB, (see Figure 7 (panels c and d) and Table 3) both TNS and PRODAN are preferably solubilized within the vesicle surface ($A_3 > A_1$ for TNS and $A_2 > A_1$ for PRODAN), as also found in the case of di-C₁₀DMAB/C₁₂EDMAB.¹⁵ In contrast, Figure 7 (panels a and b) shows that the probes are preferably housed in the hydrophobic bilayer ($A_1 > A_3$ for TNS and $A_1 > A_2$ for PRODAN) in the di-C₁₀DMAB/C₁₀TAB system (see also Table 2). The latter behavior is equivalent to that observed in the di-C₁₂DMAB/C_nTAB ($n = 10, 12$, and 14). It is interesting to notice what the latter systems have in common is that the conductivity plot shows a zigzag pattern (see Figure 3), while no zigzag is observed for the first systems, that is, di-C₁₀DMAB/C₁₄TAB and di-C₁₀DMAB/C₁₂EDMAB.¹² Again, it seems that

TABLE 4: Values of $[S]_{\text{tot}}$, κ_D , $f(\kappa_D a)$ (Calculated with eq 15), ζ , σ_{ζ} (Calculated without the Second Term of eq 16), and $\sigma_{\zeta, \text{ext}}$ (Calculated with the Whole eq 16) at Several Molar Fractions, α_1 , of the Mixed System Di- C_{10} DMAB + C_{10} TAB

α_1	$[S]_{\text{tot}}$ (mM)	$10^8 \mu_e$ ($\text{m}^2 \text{V}^{-1} \text{s}^{-1}$)	$10^9 a$ (m)	$10^{-8} \kappa_D$ (m^{-1})	$\kappa_D a$	$f(\kappa_D a)$	ζ^a (mV)	$10^3 \sigma_{\zeta}^a$ (C/m^2)	$10^3 \sigma_{\zeta, \text{ext}}^a$ (C/m^2)
0.500	7.319	4.645	16.5	2.81	4.64	1.14	78	22	25
1.000	2.427	4.166	18	1.62	2.91	1.09	73	11	14
0.200	6.393	4.698	16.5 ^b	2.63 ^b	4.33 ^b	1.13 ^b	80 ^b	21 ^b	24 ^b
0.401	6.414	4.805	16.5 ^b	2.63 ^b	6.57 ^b	1.13 ^b	82 ^b	22 ^b	25 ^b

^a Error is estimated to be <6%. ^b Calculated on the basis of an estimation of $a = 16.5$ nm. See text for the discussion.

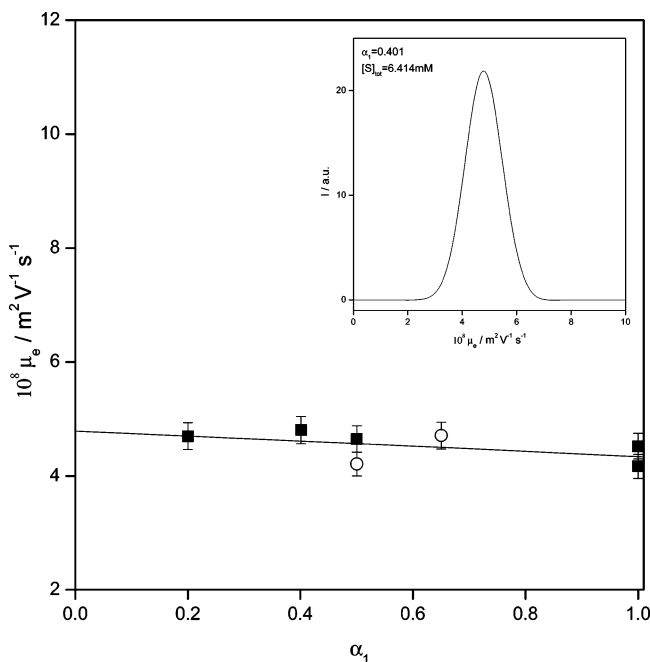


Figure 8. Plot of electrophoretic mobility μ_e as a function of molar fraction α_1 of the mixed system di- C_{10} DMAB + C_{10} TAB: vesicles (solid squares) and prevesicle aggregates (open circles). The inset shows the intensity versus electrophoretic mobility for a vesicle solution at $\alpha_1 = 0.401$ and $[S]_{\text{tot}} = 6.414$ mM. The peak is an average over 10 experimental LDE peaks.

the occurrence of this zigzag pattern, which depends on the difference between the critical concentrations CVC and CMC of the pure surfactants, as widely explained in a previous section, determines not only the behavior of CVC* versus α_1 but also the distribution of the probes within the vesicles.

The charge density on the aggregates outer surface has been evaluated by means of ζ -potential calculations, via electrophoretic mobility data. Figure 8 shows a plot of the experimental electrophoretic mobility, μ_e , as a function of the molar fraction α_1 . Each point in the graph is an average over 10 LDE experiments (see the inset, as an example), which, as can be observed in the figure, have been done at different molar fractions and at different $[S]_{\text{tot}}$. Also plotted in the figure are the results obtained for two prevesicle solutions at $\alpha_1 = 0.500$ ($[S]_{\text{tot}} = 4.733$ mM) and $\alpha_1 = 0.650$ ($[S]_{\text{tot}} = 6.504$ mM). Notice that the electrophoretic behavior of these ordered prevesicle aggregates is quite similar to that of the vesicle aggregates; this similarity has been also found when studying the emission of a fluorescent probe solubilized within both type of aggregates.¹² The well-known Henry equation has been used to relate electrophoretic mobility and ζ -potential,^{32,33} in this equation, the factor $f(\kappa_D a)$, which is called the Henry function and depends on the reciprocal Debye length, κ_D and the particle radius, a , has been estimated by the Ohshima equation,³⁵ which has been previously demonstrated¹¹ to yield much better results than the

usual approximations to Hückel and Smoluchowski limits:^{32,33}

$$f(\kappa_D a) = \left[1 + \frac{1}{2 \left(1 + \frac{2.5}{\kappa_D a (1 + 2 \exp(-\kappa_D a))} \right)^3} \right] \quad (15)$$

The size of the aggregate, a , is necessary to apply eq 15: for pure di- C_{10} DMAB vesicles and the equimolecular mixed di- C_{10} DMAB/ C_{10} TAB and/or di- C_{10} DMAB/ C_{14} TAB vesicles ($\alpha_1 = 0.5$), the values of a were taken from cryo-TEM results, previously reported in the case of the pure vesicles¹¹ or reported in this work in the case of mixed vesicles. Table 4 summarizes the experimental averaged values of μ_e , and the values of κ_D , $\kappa_D a$, $f(\kappa_D a)$, ζ -potential calculated at $\alpha_1 = 0.5$ and 1, and a given $[S]_{\text{tot}}$. For the other molar fractions studied, $\alpha_1 = 0.2$ and 0.4, the information about the vesicle size, a , is not available and consequently eq 15 is, strictly speaking, not applicable. However, we have studied the effect of the variation of a on the resulting $f(\kappa_D a)$ value. Given that in previously reported similar systems we found that the maximum variation of a with the molar fraction was around 15%, we have calculated $f(\kappa_D a)$ with eq 15 for $a = (16.5 \pm 2.5)$ nm at these two molar fractions. The results obtained yield a ζ value affected by less than 2% of relative error, which is totally masked by the intrinsic experimental error on ζ -potential calculation, which is around 5%. Thus, one can estimate an a value for the mixed system around 16.5 nm (which is the result obtained from cryo-TEM micrographies for $\alpha_1 = 0.5$) irrespectively of the molar fraction. In any case, the error on this estimation is much less than the error obtained when assuming either Hückel ($f(\kappa_D a) = 1$) or Smoluchowski ($f(\kappa_D a) = 1.5$) limits, as usually done in the literature. Table 4 also summarizes the ζ -potential values thus estimated from the experimental electrophoretic mobilities for the mixed vesicles at $\alpha_1 = 0.2$ and 0.4.

Table 4 also reports the surface charge density enclosed by the shear plane $\sigma_{\zeta, \text{ext}}$ for the molar fractions for which the vesicle size has been measured or estimated. This magnitude has been calculated, assuming a Gouy–Chapman double layer and using Löb equation:⁵³

$$\sigma_{\zeta, \text{ext}} = \frac{2\epsilon_0 \epsilon_r \kappa_D k_B T}{ze} \left[\sinh\left(\frac{ze\zeta}{2k_B T}\right) + \frac{2}{\kappa_D a} \tanh\left(\frac{ze\zeta}{4k_B T}\right) \right] \quad (16)$$

In this table, we have presented the results obtained when only the first term within the brackets of eq 16 is used, σ_{ζ} and those obtained with the whole equation, $\sigma_{\zeta, \text{ext}}$. It is worth noticing that the calculation of σ_{ζ} does not require the knowledge of vesicle size, a , while the contrary is true for the calculation of $\sigma_{\zeta, \text{ext}}$; this is the reason reduced eq 16 (without the second term) is normally used in the literature. The results listed in Table 4 deserve some remarks: (i) ζ -Potential for mixed vesicles is constant around $\zeta = 80 \pm 2$ mV, within the experimental error, with the molar fraction of the mixed system and slightly higher than the value found for pure vesicles. This value is in agreement with that one obtained for other cationic–cationic and/or

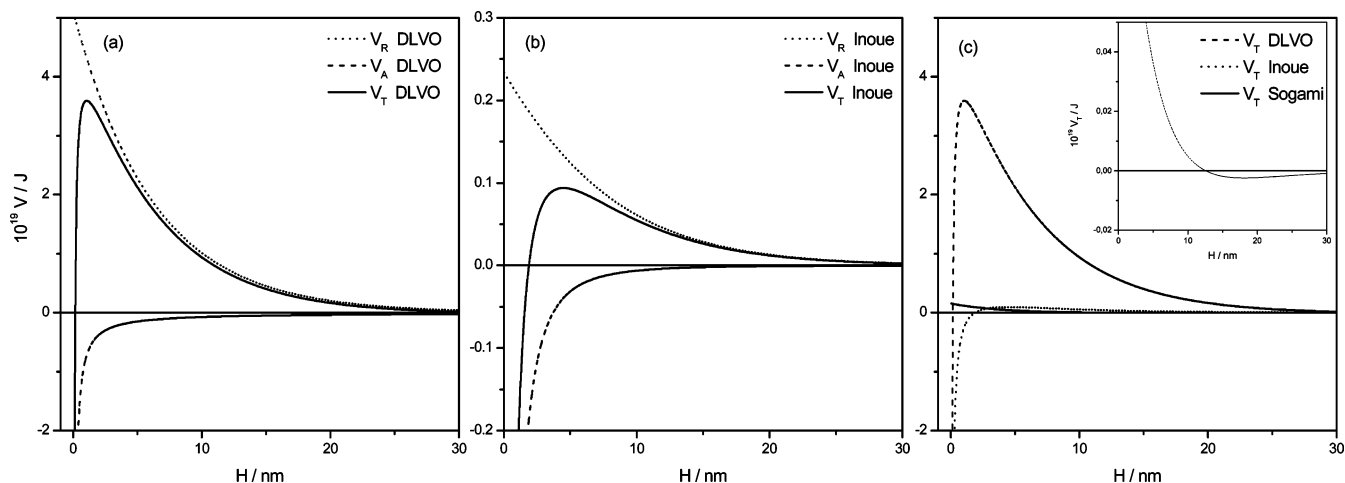


Figure 9. Plot of the total potential V_T and the attractive V_A and repulsive V_R contributions as a function of interparticle distance H obtained from (a) DLVO theory and (b) Inoue's model; (c) comparison of the results for V_T versus H , obtained from DLVO, Inoue, and Sogami models. The inset shows a zoom view of $V_{T,\text{Sogami}}$ versus H , showing the secondary minimum predicted by Sogami's model.

TABLE 5: Values of the Interaction Energy and Distance at the Energy Barrier, $V_{T,\text{Max}}$ and H_{Max} , and/or at the Secondary Minimum, $V_{T,\text{min}}$ and H_{min} , of the DLVO Theory, the Theoretical Models of Inoue and Sogami, and the Combinations Thereof, Applied to Pure Di- C_{10}DMAB and Mixed Di- $\text{C}_{10}\text{DMAB} + \text{C}_{10}\text{TAB}$ Vesicles at Different Molar Fractions, α_1 , of the System

α_1	[S] _{tot} (mM)	DLVO's theory		Inoue's model		Sogami's model		DLVO–Sogami's model		Inoue–Sogami's model	
		$10^{19}V_{T,\text{max}}$ (J)	H_{max} (nm)	$10^{21}V_{T,\text{max}}$ (J)	H_{max} (nm)	$10^{22}V_{T,\text{min}}$ (J)	H_{min} (nm)	$10^{19}V_{T,\text{max}}$ (J)	H_{max} (nm)	$10^{21}V_{T,\text{max}}$ (J)	H_{max} (nm)
0.200	6.393	3.2	0.8	6.6	3.7	−2.6	11	3.3	0.8	10	2.9
0.401	6.414	3.2	0.8	7.1	3.7	−2.7	11	3.3	0.8	10	2.9
0.500	7.319	3.1	0.8	5.5	3.8	−2.4	10	3.1	0.8	8	3.0
1	2.427	3.6	1.0	9.4	4.5	−2.4	18	3.7	1.0	15	3.4

cationic–nonionic mixed vesicles, previously studied in our laboratory,^{9–12,15} indicating that is the ionic polar head of the dialkylsurfactant which govern the ζ -potential of the interface. (ii) Surface charge density of the mixed vesicles is also constant around $\sigma_{\zeta,\text{ext}} = (24 \pm 2) \times 10^{-3} \text{ C/m}^2$ independently of the molar fraction but higher than this value for the pure vesicles, $\sigma_{\zeta,\text{ext}} = (14 \pm 1) \times 10^{-3} \text{ C/m}^2$, because of the difference on the particle size. (iii) The difference among σ_{ζ} and $\sigma_{\zeta,\text{ext}}$ is around 8–10%, higher than the error on the magnitude, confirming that the second term of eq 16 must be considered.

From a theoretical point of view, we have applied to the systems studied in this work the original DLVO theory, and also the Inoue and Sogami models, that try to improve DLVO predictions. Also included in this work is the same theoretical analysis for other pure and mixed cationic vesicles of the family di- $\text{C}_m\text{DMAB} + \text{C}_n\text{TAB}$ ($m = 10, 12$ and $n = 10, 12$, and 14) whose experimental study had been also done in our laboratory.^{9,12,15} For that purpose, calculations have been made by using the equations listed in the theoretical overview, where all the magnitudes are already defined with the exception of ψ_0 , which has been substituted by the experimental ζ -potential in each case, as usually done in this type of calculations.^{32,33} A Hamaker constant of $5 \times 10^{-20} \text{ J}$, estimated from the values found in the literature for similar systems,^{6,34,54–56} has been used to compute the van der Waals contribution to the interaction energy.

Figure 9 (panels a and b) shows, as an example, the repulsive V_R , attractive V_A , and total interaction energies V_T as a function of the distance H obtained by the DLVO theory and the Inoue's model for the binary di- $\text{C}_{10}\text{DMAB}/\text{H}_2\text{O}$ system. Both models yield similar trends, as can be seen in the figure, with a primary minimum at very short distances ($H \rightarrow 0$) and an energy barrier, but without a secondary minimum. The existence of an energy barrier confirms the stability of the system, avoiding particle

coagulation, in agreement with experimental evidences. Note (see Table 5, $\alpha_1 = 1$, last line) that the energy barrier is higher ($V_{T,\text{max}} \approx 10^{-19} \text{ J}$) and appears at shorter distances (H_{max} around 1 nm) when applying DLVO theory than in the case of Inoue's model ($V_{T,\text{max}} \approx 10^{-21} \text{ J}$ and H_{max} around 4.5 nm). Furthermore, the attractive contribution to the total interaction energy has less importance in DLVO theory ($V_R \approx 5.5 V_A$) than it has in Inoue's model ($V_R \approx 3 V_A$). Figure 9c shows the total interaction energy obtained with the three theories, DLVO, Inoue, and Sogami for di- C_{10}DMAB vesicles. It can be seen that Sogami's model, developed for medium-to-long distances, predicts total energy values much less than the other models ($V_{T,\text{DLVO}} \approx 30 V_{T,\text{Inoue}} \approx 10^2 V_{T,\text{Sogami}}$) and an energy minimum at longer distances ($H \approx 18 \text{ nm}$) that would be pointing to a flocculation regime in the medium distance range (see also Table 5, $\alpha_1 = 1$).

Figure 10 (panels a–c) summarizes, as an example, the total interaction energy predicted by the three models, for the mixed di- $\text{C}_{10}\text{DMAB}/\text{C}_{10}\text{TAB}$ vesicles at the molar fractions α_1 studied in the experimental part of this work. The energy and distance values at the energy barrier and/or at the secondary minimum have been reported for this system (Table 5) and in the case of previously reported systems (Tables 6–9). In view of Figure 10 (panels a and b) and Tables 5–9, several general conclusions regarding DLVO and Inoue models, valid at any distance H , can be made: (i) An energy barrier at H_{max} is predicted at around 1 nm with the DLVO theory and at around 4–5 nm with the Inoue's model for all the systems at any composition. Both distance values are much lower than vesicles size. Furthermore, no secondary minimum appears, revealing the total absence of flocculation phenomena. (ii) The energy barrier (higher again with DLVO) seems unaffected by the molar fraction, α_1 , with the only exception being that of the systems for which pure vesicles are clearly smaller than mixed vesicles. On the other

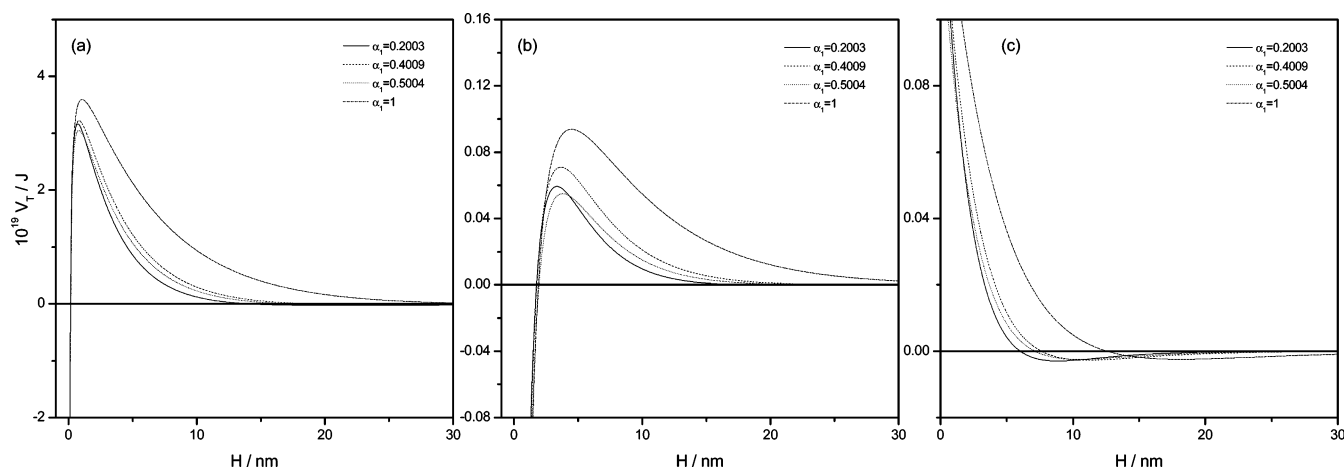


Figure 10. Plot of V_T versus H for the mixed diC₁₀DMAB + C₁₀TAB vesicles at different molar fractions α_1 obtained from (a) DLVO; (b) Inoue; and (c) Sogami theoretical models.

TABLE 6: Values of the Interaction Energy and Distance at the Energy Barrier, $V_{T,\text{Max}}$ and H_{Max} , and/or at the Secondary Minimum, $V_{T,\text{min}}$ and H_{min} , of the DLVO Theory, the Theoretical Models of Inoue and Sogami, and the Combinations Thereof, Applied to Pure Di-C₁₀DMAB and Mixed Di-C₁₀DMAB + C₁₂EDMAB Vesicles at Different Molar Fractions, α_1 , of the System

α_1	[S] _{tot} (mM)	DLVO's theory		Inoue's model		Sogami's model		DLVO–Sogami's model		Inoue–Sogami's model	
		$10^{19}V_{T,\text{max}}$ (J)	H_{max} (nm)	$10^{21}V_{T,\text{max}}$ (J)	H_{max} (nm)	$10^{22}V_{T,\text{min}}$ (J)	H_{min} (nm)	$10^{19}V_{T,\text{max}}$ (J)	H_{max} (nm)	$10^{21}V_{T,\text{max}}$ (J)	H_{max} (nm)
0.210	4.531	9.2	0.9	17	4.4	−6.2	13	9.4	0.9	24	3.6
0.300	4.477	8.5	0.9	13	4.8	−5.3	13	8.7	0.9	18	4.0
0.400	4.498	8.2	0.9	11	5.0	−4.9	13	8.4	0.9	15	4.1
0.500	4.510	8.0	0.9	10	5.2	−4.6	13	8.1	0.9	13	4.3
0.749	4.514	8.1	0.9	11	5.1	−4.8	13	8.3	0.9	14	4.2
0.849	4.481	9.1	0.9	17	4.5	−6.1	14	9.3	0.9	23	3.7
0.849	3.607	8.5	1.0	14	5.0	−5.0	15	8.6	1.0	18	4.7
1	2.427	3.6	1.0	9.4	4.5	−2.4	18	3.7	1.0	15	3.4

TABLE 7: Values of the Interaction Energy and Distance at the Energy Barrier, $V_{T,\text{Max}}$ and H_{Max} , and/or at the Secondary Minimum, $V_{T,\text{min}}$ and H_{min} , of the DLVO Theory, the Theoretical Models of Inoue and Sogami, and the Combinations Thereof, Applied to Pure Di-C₁₂DMAB and Mixed Di-C₁₂DMAB + C₁₀TAB Vesicles at Different Molar Fractions, α_1 , of the System

α_1	[S] _{tot} (mM)	DLVO's theory		Inoue's model		Sogami's model		DLVO–Sogami's model		Inoue–Sogami's model	
		$10^{19}V_{T,\text{max}}$ (J)	H_{max} (nm)	$10^{21}V_{T,\text{max}}$ (J)	H_{max} (nm)	$10^{22}V_{T,\text{min}}$ (J)	H_{min} (nm)	$10^{19}V_{T,\text{max}}$ (J)	H_{max} (nm)	$10^{21}V_{T,\text{max}}$ (J)	H_{max} (nm)
0.200	0.797	4.6	1.3	20	4.7	−2.9	33	4.8	1.2	36	3.1
0.401	1.097	4.4	1.2	17	4.6	−2.9	28	4.6	1.2	29	3.2
0.500	1.458	4.3	1.1	16	4.4	−3.1	24	4.5	1.1	27	3.1
0.647	1.904	4.1	1.1	13	4.5	−2.8	21	4.2	1.0	20	3.3
0.847	2.145	3.8	1.1	11	4.5	−2.6	19	4.0	1.0	17	3.4
1	0.305	4.7	1.6	24	5.2			5.1	1.5	55	3.0

TABLE 8: Values of the Interaction Energy and Distance at the Energy Barrier, $V_{T,\text{Max}}$ and H_{Max} , and/or at the Secondary Minimum, $V_{T,\text{min}}$ and H_{min} , of the DLVO Theory, the Theoretical Models of Inoue and Sogami, and the Combinations Thereof, Applied to Pure Di-C₁₂DMAB and Mixed Di-C₁₂DMAB + C₁₂EDMAB Vesicles at Different Molar Fractions, α_1 , of the System

α_1	[S] _{tot} (mM)	DLVO's theory		Inoue's model		Sogami's model		DLVO–Sogami's model		Inoue–Sogami's model	
		$10^{19}V_{T,\text{max}}$ (J)	H_{max} (nm)	$10^{21}V_{T,\text{max}}$ (J)	H_{max} (nm)	$10^{22}V_{T,\text{min}}$ (J)	H_{min} (nm)	$10^{19}V_{T,\text{max}}$ (J)	H_{max} (nm)	$10^{21}V_{T,\text{max}}$ (J)	H_{max} (nm)
0.202	1.497	23	1.1	71	5.0	−15	23	24	1.1	97	4.0
0.202	0.931	24	1.2	80	5.3	−15	29	24	1.2	112	4.3
0.384	1.402	21	1.2	59	5.2	−13	24	21	1.1	82	4.3
0.384	0.872	23	1.3	78	5.4	−14	30	23	1.2	109	4.3
0.478	1.541	19	1.2	44	5.6	−10	23	19	1.2	60	4.6
0.478	0.959	20	1.3	54	5.8	−11	29	20	1.3	75	4.7
0.581	1.118	20	1.2	58	5.4	−12	27	20	1.2	81	4.4
0.588	0.957	21	1.3	68	5.4	−13	29	21	1.2	94	4.3
0.798	1.467	18	1.2	47	5.3	−11	24	18	1.1	65	4.3
1	0.305	4.7	1.6	24	5.2			5.1	1.5	55	3.0

hand, Sogami's model predicts a minimum for all the systems, irrespective of the molar fraction, α_1 , at longer distances ($H_{\text{min}} \approx 10\text{--}30$ nm). This minimum is characterized by a very low stabilization energy, much lower than that found for latex dispersions.²⁶ Additionally, it is noticeable that the distance at

which the secondary minimum, H_{min} , of the vesicles theoretically studied in this work appears is 1 order of magnitude lower than that of the above-mentioned latex dispersions.²⁶

Figure 11 (a–c) summarizes the total interaction energy predicted by the three models for the vesicles studied in this

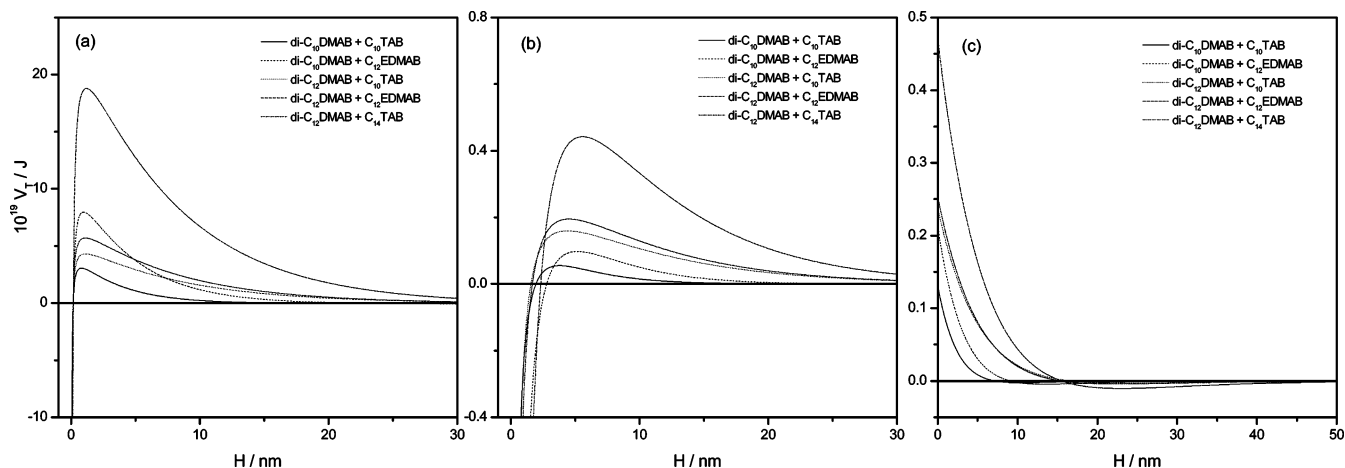


Figure 11. Plot of V_T versus H for mixed $\text{di-C}_m\text{DMAB} + \text{C}_n\text{TAB}$ vesicles ($m = 10$ and 12 and $n = 10, 12$, and 14) at the equimolar composition, $\alpha_1 = 0.5$, obtained from (a) DLVO; (b) Inoue; and (c) Sogami theoretical models.

TABLE 9: Values of the Interaction Energy and Distance at the Energy Barrier, $V_{T,\text{Max}}$ and H_{Max} , and/or at the Secondary Minimum, $V_{T,\text{min}}$ and H_{min} , of the DLVO Theory, the Theoretical Models of Inoue and Sogami, and the Combinations Thereof, Applied to Pure $\text{Di-C}_{12}\text{DMAB}$ and Mixed $\text{Di-C}_{12}\text{DMAB} + \text{C}_{14}\text{TAB}$ Vesicles at Different Molar Fractions, α_1 , of the System

α_1	[S] _{tot} (mM)	DLVO's theory		Inoue's model		Sogami's model		DLVO–Sogami's model		Inoue–Sogami's model	
		$10^{19}V_{T,\text{max}}$ (J)	H_{max} (nm)	$10^{21}V_{T,\text{max}}$ (J)	H_{max} (nm)	$10^{22}V_{T,\text{min}}$ (J)	H_{min} (nm)	$10^{19}V_{T,\text{max}}$ (J)	H_{max} (nm)	$10^{21}V_{T,\text{max}}$ (J)	H_{max} (nm)
0.196	1.001	6.3	1.2	28	4.5	−5.0	28	6.6	1.1	45	3.2
0.196	0.626	6.2	1.3	25	5.1	−4.0	37	6.4	1.3	44	3.5
0.396	1.283	6.1	1.1	24	4.4	−4.7	25	6.3	1.1	39	3.2
0.396	0.800	5.8	1.3	21	5.1	3.8	32	6.1	1.3	36	3.7
0.496	1.591	5.7	1.1	20	4.5	−4.2	22	5.9	1.1	30	3.4
0.496	0.996	5.7	1.2	20	5.0	−3.8	29	6.0	1.2	33	3.6
0.651	2.338	5.6	1.0	19	4.2	−4.4	18	5.8	1.0	28	3.2
0.651	1.461	5.4	1.1	17	4.9	−3.6	23	5.6	1.1	26	3.7
0.751	1.951	5.0	1.1	12	5.0	−3.1	20	5.1	1.1	18	3.8
0.849	2.905	5.0	1.0	12	4.5	−3.5	17	5.2	1.0	18	3.5
1	0.305	4.7	1.6	24	5.2			5.1	1.5	55	3.0

work and those previously reported by us, at $\alpha_1 = 0.5$. Each model predicts V_T values which are very similar for all the systems, irrespective of the double-chain ($\text{di-C}_{10}\text{DMAB}$ or $\text{di-C}_{12}\text{DMAB}$) and/or single-chain (C_nTAB , $n = 10, 12, 14$) surfactant. The only exception to the above cited conclusion is the system $\text{di-C}_{12}\text{DMAB}/\text{C}_{12}\text{EDMAB}$, which was the first mixed vesicle system studied and reported by our group.⁹ These vesicles are bigger than the others, this fact being attributed to the combined effect of (i) a bigger polar head on the single-chain surfactant (EDMA^+ with respect to TMA^+) and (ii) a different experimental protocol of vesicle preparation involving less sonication.

As described above, Sogami's model only considers the electrostatic interaction (repulsive and attractive) at medium-to-long distances. For that reason, the predictions of the Sogami's model are far away from those of DLVO and Inoue's models. The Sogami's model was developed to analyze particle interactions within a range of distances that are longer than those used in the above-mentioned theoretical colloidal models. In this work, we have proposed a more general model that takes into account the interaction between particles (i.e. vesicles) at short and medium-to-long distances. For that purpose, we have combined the electrostatic potential at medium-long distances proposed by Sogami (eq 11) with the total potential at any distance proposed by DLVO (eq 1) or Inoue's (eq 8) model in order to estimate the total interaction energy between vesicles. Thus, the total interaction $V_T(H)$ between two spherical particles (i.e., vesicles) of equal radius a and at a distance H can be obtained considering a DLVO–Sogami potential (eq 17), or a

Inoue–Sogami potential (eq 18), respectively, as follows:

$$V_T(H) = \frac{(Ze)^2}{\epsilon} \left[\frac{\sinh(\kappa_D a)}{\kappa_D a} \right]^2 [1 + \kappa_D a \coth(\kappa_D a) - \frac{1}{2} \kappa_D (H + 2a) \frac{\exp[-\kappa_D (H + 2a)]}{(H + 2a)} + \frac{64\pi a^0 k_B T}{\kappa_D^2} \Gamma^2 \exp(-\kappa_D H) - \frac{Aa}{12H}] \quad (17)$$

or

$$V_T(H) = \frac{(Ze)^2}{\epsilon} \left[\frac{\sinh(\kappa_D a)}{\kappa_D a} \right]^2 [1 + \kappa_D a \coth(\kappa_D a) - \frac{1}{2} \kappa_D (H + 2a) \frac{\exp[-\kappa_D (H + 2a)]}{(H + 2a)} + \frac{\epsilon a \psi_0^2}{2} \ln[1 + \exp(-\kappa_D H)] - \frac{A_{232}}{12} (F_{11} + F_{22} - 2F_{12})] \quad (18)$$

which can be easily derived from eqs 1 and 8 (to build eq 17) and eqs 1 and 11 (to build eq 18).

Tables 5–9 report all the results obtained when applying both extended models to the vesicles previously studied with DLVO, Inoue, and Sogami models, at several molar fractions. A plot of V_T versus H for those systems at the equimolar composition is shown in Figure 12. Comparing either Figure 11a with Figure 12a or the results reported in Tables 5–9, it can be deduced that the inclusion of Sogami's electrostatic potential

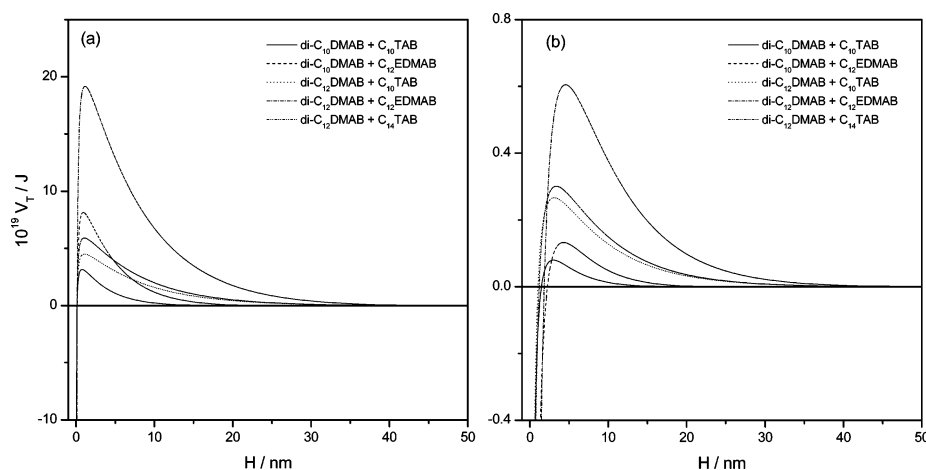


Figure 12. Plot of V_T versus H for mixed $\text{di-C}_m\text{DMAB} + \text{C}_n\text{TAB}$ vesicles ($m = 10$ and 12 and $n = 10, 12$, and 14) at the equimolecular composition, $\alpha_1 = 0.5$, obtained from (a) extended DLVO–Sogami model; and (b) extended Inoue–Sogami model.

at medium-to-long distances in the DLVO theory does not almost modify V_T , $V_{T,\max}$, or H_{\max} values, and accordingly all the corresponding conclusions previously commented for the DLVO theory remain unaffected. This is due to the fact that $V_{T,\text{Sogami}}$ is less than 1% of the DLVO potential. The minimum predicted by the Sogami's model at medium distances disappears when using the extended DLVO–Sogami model. However, when the results obtained with Inoue's model (Figure 11b) are compared with those yielded by the Inoue–Sogami model (Figure 12b) (see also Tables 5–9), appreciable differences can be observed: V_T and $V_{T,\max}$ are 30% higher with this extended model. The position of the energy barrier, H_{\max} , is also affected, being shifted around 30% toward shorter distances (3–4 nm). Even then, both parameters, $V_{T,\max}$ and H_{\max} , are higher in all the systems than those predicted by the DLVO theory. With respect to the secondary minimum found at medium distances with the Sogami model, it is noticeable that it also disappears with the Inoue–Sogami model. It seems that this extended model yields slightly different results depending on the length of the double-chain surfactant, $\text{di-C}_{10}\text{DMAB}$ or $\text{di-C}_{12}\text{DMAB}$, since the equimolecular mixtures of $\text{di-C}_{10}\text{DMAB}/\text{C}_n\text{TAB}$ ($n = 10, 12, 14$) show a slightly lower total interaction energy than those of $\text{di-C}_{12}\text{DMAB}/\text{C}_n\text{TAB}$. On the other hand, irrespective of the theoretical potential used, the $\text{di-C}_{12}\text{DMAB} + \text{C}_{12}\text{-EDMAB}$ system is the only one which shows positive deviations with respect to the behavior of the other mixed systems analyzed in this work, confirming that the vesicle size, which appears in eqs 1, 8, 11, 17, and 18, has an important effect on the calculation of the total interaction energy, being dominant over other factors, such as the composition of the system, α_1 , or the ζ -potential.

Conclusions

According to this and previous related works, the main features of mixed colloidal systems constituted by a cationic double-chain and a cationic single-chain surfactant, belonging to the dialkyldimethyl- and alkyltrimethylammonium bromide families, respectively, can be briefly summarized as follows. These mixtures lead to the formation of prevesicle and vesicle aggregates on the very diluted concentration range, within which two critical aggregation concentrations are found: the mixed critical aggregate concentration CAC^* and the mixed critical vesicle concentration CVC^* . Different kind of nanoaggregates can be found in the regions limited by these critical concentrations: (i) disordered prevesicle aggregates, with a variety of

sizes and shapes, at concentrations below CAC^* ; (ii) ordered prevesicle aggregates, with a clear onion-type aggregation pattern, at concentrations between CAC^* and CVC^* ; and (iii) vesicles at concentrations above CVC^* , which are unilamellar and spherical with a medium polydispersity and a net averaged surface density charge of around 14×10^{-3} (pure $\text{di-C}_{10}\text{DMAB}$ vesicles) and $24 \times 10^{-3} \text{ C m}^{-2}$ ($\text{di-C}_{10}\text{DMAB}/\text{C}_n\text{TAB}$ mixed vesicles, $n = 10$ or 14). The presence of all the abovementioned concentration domains is directly correlated with typical zigzag conductivity plots. Two main behaviors can be identified for these bicationic mixed colloidal systems: that of those systems that show a clear zigzag pattern in the conductivity plot and that of the systems without this zigzag. Its occurrence and the consequences on the aggregation patterns and characteristics depend on the difference among the CVC and CMC values of the pure double-chain and single-chain surfactants, respectively: the zigzag is detected only when these critical concentrations are enough separated. Both prevesicle and vesicle aggregates offer three microenvironments where fluorescence probes, as TNS and PRODAN, may be housed: (i) disordered prevesicles, λ (inside) $< \lambda$ (within clusters) $< \lambda$ (bulk), for TNS and PRODAN; and (ii) ordered prevesicles or vesicles, λ (bilayer) $< \lambda$ (bulk) $< \lambda$ (surface) for TNS and λ (bilayer) $< \lambda$ (surface) $< \lambda$ (bulk) for PRODAN. Additionally, the spectroscopic study indicates that the hydrophobicities of the lipidic bilayer and the surface of the vesicles studied in this work resemble those of media with dielectric constants of around 30 and 75, respectively. The theoretical predictions yielded by DLVO theory and Inoue's model point to the existence of a primary minimum at very short distances and an energy barrier, but without a secondary minimum, avoiding particle coagulation and, thus, confirming the stability of the pure and mixed vesicles, in agreement with experimental evidences. On the other hand, Sogami's model predicts a minimum for all the systems, irrespective of the molar fraction α_1 at longer distances that would be pointing to a flocculation regime in the medium-distance range. It can be concluded that, general and qualitatively speaking, the models proposed by Inoue, Sogami, or even the extended DLVO–Sogami, and Inoue–Sogami models, do not significantly improve the theoretical predictions of diluted vesicle systems with respect to those of the classical DLVO theory. However, it is remarkable that the extended models analyzed in this work have the advantage of being applicable in a wide range of interparticle distances, which means that there

is an allowance for the characterization of diluted or even medium concentrated vesicle systems.

Acknowledgment. The authors thank the Spanish Ministry of Education, Project No. CTQ2005-1106. O.L. thanks MEC of Spain (Project No. SAF2005-00775) for supporting TEM and cryo-TEM measurements.

References and Notes

- (1) Christian, S. D.; Scamehorn, J. F. *Solubilization in Surfactant Aggregates*; Marcel Dekker: New York, 1995; Vol. 55.
- (2) Holland, P. M.; Rubingh, D. N. *Mixed Surfactant Systems*; American Chemical Society: Washington, DC, 1992.
- (3) Rosoff, M. *Vesicles*; Marcel Dekker: New York, 1996.
- (4) Somasundaran, P.; Hubbard, A. *Encyclopedia of Surface and Colloid Science*; Marcel Dekker: Santa Barbara, CA, 2002.
- (5) Tanford, C. *The Hydrophobic Effect: Formation of Micelles and Biological Membranes*; Wiley & Sons: New York, 1980.
- (6) Kawasaki, H.; Imahayashi, R.; Tanaka, S.; Almgren, M.; Karlsson, G.; Maeda, H. *J. Phys. Chem. B* **2003**, *107*, 8661.
- (7) Lichtenberg, D.; Robson, R. J.; Dennis, E. A. *Biochim. Biophys. Acta* **1983**, *737*, 285.
- (8) Lichtenberg, D. *Biochim. Biophys. Acta* **1985**, *821*, 470.
- (9) Junquera, E.; Arranz, R.; Aicart, E. *Langmuir* **2004**, *20*, 6619.
- (10) Junquera, E.; del Burgo, P.; Arranz, R.; Llorca, O.; Aicart, E. *Langmuir* **2005**, *21*, 1795.
- (11) Junquera, E.; del Burgo, P.; Boskovic, J.; Aicart, E. *Langmuir* **2005**, *21*, 7143.
- (12) Aicart, E.; del Burgo, P.; Llorca, O.; Junquera, E. *Langmuir* **2006**, *22*, 4027.
- (13) Niu, S.; Gopidas, K. R.; Turro, N. J.; Gabor, G. *Langmuir* **1992**, *8*, 1271.
- (14) Karukstis, K. K.; Savin, D. A.; Loftus, C. T.; D'Angelo, N. D. *J. Colloid Interface Sci.* **1998**, *203*, 157.
- (15) del Burgo, P.; Aicart, E.; Junquera, E. *Colloids Surf. A* **2006**, in press.
- (16) Chesnoy, S.; Huang, L. *Annu. Rev. Biophys. Biomol. Struct.* **2000**, *29*, 27.
- (17) Huebner, S.; Battersby, B. J.; Grimm, R.; Cevc, G. *Biophys. J.* **1999**, *76*, 3158.
- (18) Mel'nikova, Y. S.; Mel'nikov, S. M.; Lofroth, J. E. *Biophys. Chem.* **1999**, *81*, 125.
- (19) Tarahovsky, Y. S.; Rakhmanova, V. A.; Epand, R. M.; MacDonald, R. C. *Biophys. J.* **2002**, *82*, 264.
- (20) Aguirrezabala, X.; Martin-Benito, J.; Caston, J. R.; Miranda, R.; Valpuesta, J. M.; Carrascosa, J. L. *EMBO J.* **2005**, *24*, 3820.
- (21) Argy, G.; Bricout, F.; d'Hermies, F.; Cheymol, A. C. *R. Acad. Sci., Ser. III* **1999**, *322*, 863.
- (22) Budavari, S. *The Merck Index*; Merck & Co., Inc.: Whitehouse Station, NJ, 1996.
- (23) Derjaguin, B. V.; Landau, L. *Acta Physicochim.* **1941**, *14*, 633.
- (24) Verwey, E. J. W.; Overbeek, J. T. G. *Theory of the Stability of Lyophobic Colloids*; Elsevier: Amsterdam, The Netherlands, 1948.
- (25) Minami, H.; Inoue, T.; Shimozaawa, R. *J. Colloid Interface Sci.* **1993**, *158*, 460.
- (26) Sogami, I.; Ise, N. *J. Chem. Phys.* **1984**, *81*, 6320.
- (27) Junquera, E.; Aicart, E. *Rev. Sci. Instrum.* **1994**, *65*, 2672.
- (28) Kunitake, T.; Okahata, Y. *J. Am. Chem. Soc.* **1980**, *102*, 549.
- (29) Dubochet, J.; Adrian, M.; Chang, J. J.; Homo, J. C.; Lepault, J.; McDowell, A. W.; Schultz, P. Q. *Rev. Biophys.* **1988**, *21*, 129.
- (30) Llorca, O.; McCormack, E.; Hynes, G.; Grantham, J.; Cordell, J.; Carrascosa, J. L.; Willison, K. R.; Fernández, J. J.; Valpuesta, J. M. *Nature* **1999**, *402*, 693.
- (31) Junquera, E.; Peña, L.; Aicart, E. *Langmuir* **1997**, *13*, 219.
- (32) Delgado, A. V. *Interfacial Electrokinetics and Electrophoresis*; Marcel Dekker: New York, 2002; Vol. 106.
- (33) Hunter, R. J. *Zeta Potential in Colloids Science. Principles and Applications*; Academic Press: London, 1981.
- (34) Israelachvili, J. *Intermolecular and Surface Forces with Application to Colloidal and Biological Systems*; Academic Press: London, 1985.
- (35) Ohshima, H.; Furusawa, K. *Electrical Phenomena at Interfaces. Fundamentals, Measurements, and Applications*; Marcel Dekker: New York, 1998.
- (36) Hamaker, H. C. *Physica* **1937**, *4*, 1058.
- (37) Hogg, R.; Healy, T. W.; Fuerstenau, D. W. *Trans. Faraday Soc.* **1966**, *62*, 1638.
- (38) Vold, M. J. *J. Colloid Sci.* **1961**, *19*, 1.
- (39) Sogami, I. *Phys. Lett. A* **1983**, *96*, 199.
- (40) Phillips, J. N. *Trans. Faraday Soc.* **1955**, *51*, 561.
- (41) Safinya, C. R. *Curr. Opin. Struct. Biol.* **2001**, *11*, 440.
- (42) Tarahovsky, Y. S.; Arsenaault, A. L.; MacDonald, R. C.; McIntosh, T. J.; Epand, R. M. *Biophys. J.* **2000**, *79*, 3193.
- (43) Karukstis, K. K. Encapsulation of Fluorophores in Multiple Microenvironments. In *Surfactant-Based Supramolecular Assemblies*; Nanostructured Materials, Micelles and Colloids, Vol. 3; Academic Press: London, 2001.
- (44) Lakowicz, J. R. *Principles of Fluorescence Spectroscopy*; Kluwer Academic/Plenum: New York, 1999.
- (45) Karukstis, K. K.; McCormack, S. A.; McQueen, T. M.; Goto, K. F. *Langmuir* **2004**, *20*, 64.
- (46) Lobo, B. C.; Abelt, C. J. *J. Phys. Chem. A* **2003**, *107*, 10938.
- (47) Parusel, A. B.; Nowak, W.; Grimme, S.; Köhler, G. *J. Phys. Chem.* **1998**, *102*, 7149.
- (48) Rettig, W.; Paeplow, B.; Herbst, H.; Mullen, K.; Desvergne, J. P.; Bouas-Laurent, H. *New J. Chem.* **1999**, *23*, 453.
- (49) Zachariasse, K. A.; Grobys, M.; van der Haar, T.; Hebecker, A.; Il'ichev, Y. V.; Morawski, O.; Riicker, I.; Kihlne, W. *J. Photochem. Photobiol. A* **1997**, *105*, 373.
- (50) Karukstis, K. K.; Zieleniuk, C. A.; Fox, M. J. *Langmuir* **2003**, *19*, 10054.
- (51) del Burgo, P.; Aicart, E.; Junquera, E. *Appl. Spectrosc.* **2006**, in press.
- (52) Lide, D. R. *CRC Handbook of Chemistry and Physics*; CRC Press: Boca Raton, 2004.
- (53) Loeb, A. L.; Overbeek, J. T. G.; Wiersema, P. H. *The Electrical Double Layer around a Spherical Colloid Particle*; MIT Press: Cambridge, MA, 1961.
- (54) Gamon, B. L.; Virden, J. W.; Berg, J. C. *J. Colloid Interface Sci.* **1989**, *132*, 125.
- (55) Hough, D. B.; White, L. R. *Adv. Colloid Interface Sci.* **1980**, *14*, 3.
- (56) Visser, J. *Adv. Colloid Interface Sci.* **1972**, *3*, 331.